University of Bath

Alternative formats
If you require this document in an alternative format, please contact:
openaccess@bath.ac.uk

WILEY-VCH

Thermally Reduced Graphene Oxide Nanohybrids of Chiral Functional Naphthalenediimides for Prostate Cancer Cells Bioimaging

James A. Tyson,[a] Vincenzo Mirabello,[a]* David G. Calatayud,[a] Haobo Ge,[a] Gabriele Kociok-Köhn,[b] Stanley W. Botchway,[c] G. Dan Pantoş,[a]* Sofia I. Pascu[a]*

Dr. Sofia I. Pascu, Dr. G. Dan Pantoş, Dr. Vincenzo Mirabello, J. A. Tyson, Dr. David G. Calatayud, Dr. Haobo Ge

a. Department of Chemistry, University of Bath, Claverton Down, BA2 7AY, UK

Dr. Gabriele Kociok-Köhn

b. Chemical Characterisation and Analysis Facility (CCAF), University of Bath, Claverton Down, BA2 7AY, UK

Prof. Stanley W. Botchway

b. Central Laser Facility, Rutherford Appleton Laboratory, Research Complex at Harwell, STFC Didcot OX11 0QX, UK

E-mail: v.mirabello@bath.ac.uk, g.d.pantos@bath.ac.uk, s.pascu@bath.ac.uk

We report on the supramolecular assemblies formed between planar carbon systems (PCS) such as thermally reduced graphene oxide (TRGO) and its small-molecule model system coronene and a series of D- and L- α amino acid derivatized naphthalenediimides (NDIs) where the halogen substituents (X =F, Cl, Br, I) were varied systematically. Confocal fluorescence microscopy of NDIs, NDI-coronene and NDI-TRGO complexes was performed proving the uptake and stability of such complexes in the cellular environment and suggesting their potential as prostate cancer imaging agents. ^{1}H NMR and UV-Vis spectroscopy studies support the formation of charge transfer complexes whereby the increasing polarizability and general electronegativity of the aryl halide-substituted at the NDI periphery influences the magnitude of the association constants in the ground state between NDI and coronene. Complexation between NDIs and planar carbon systems also results in stable photoexcited

1

assemblies within the solution (coronene) as well as the dispersed phased (TRGO). Fluorescence emission titrations and 2-photon time correlated single photon counting (TCSPC) measurements suggest the existence of dynamic quenching mechanisms upon the excitation of the fluorophore in the presence of the carbon substrates, as these methods are sensitive proves for the subtle changes in the NDIs environment. The series of halogenated species used exerts supramolecular control over the degree of surface assembly on the TRGO and over the interactions with the coronene molecule, and this is of relevance to the assembly of future biosensing platforms as these materials can both be viewed as congeners of graphene. Finally MTT assays carried out in PC-3 cells demonstrate that the stable noncovalent functionalization of TRGO and coronene with either L or D NDIs remarkably improves the cellular viability in the presence of such graphene-like materials. These phenomena are of particular relevance for the understanding of the direct donor-acceptor interactions in solution which govern the design of nano-materials with future biosensing and bioimaging applications.

1. Introduction

Several recently-discovered allotropes of carbon such as fullerenes, carbon nanotubes (CNTs), graphene and its functionalised derivatives such as graphene oxides have garnered considerable interest over recent years.[1] Graphene excites the imagination of lab-based chemists due to its many impressive properties such as high intrinsic mobility (200, 000 cm^2/Vs),[2] high thermal (5000 Wm−1K −1), electrical conductivity,[3] high Young's modulus (1.0 TPa)[4] and high optical transmittance (97.7%).[5] Since its discovery it has become a highly promising material with envisaged applications ranging from biosensors,[6] high performance electronics,[7] photovoltaics and composite materials.[8] However, one of the key challenges in advancing the graphene based technologies remains in the area of effective surface functionalization and the formation of stable hybrid graphene-based functional

materials which are amenable to surface modifications in a sustainable and straight forward manner accessible to standard chemistry laboratories. The difficulties surrounding the lab-scale availability of functional graphenes are associated with a considerable structural and atomic variability of the bulk-produced materials. Recently, to bypass these limitations the use of GO and of its thermally reduced variant, TRGO, has emerged.[9, 10] The functionalization of carbon-based nanomaterials, especially CNTs and graphene, is extremely attractive in the bioanalytical area for electrode design as they can combine properties of the high surface area, acceptable biocompatibility, chemical and electrochemical stability and good electrical conductivity.[11],[12] For instance, CNTs demonstrate faster response time and higher sensitivity than traditional electrodes. Such improved performance is attributed to their one-dimensional hollow tubular nano-chemistry that is responsible for the efficient capture and promotion of electron transfer from analytes.[13] Marquette *et. al*. demonstrated a method to enhance the chemio luminescent properties of an on-chip biosensor for the detection of protein and oligonucleotides. Such enhancement is associated with the use of carbon microarray and consequently increase of specific surface area for the probe biomolecule immobilization.[14]

Popular methods of carbon planar surface modification rely on covalent approaches that require oxidised variants of graphene as a prerequisite to introducing various oxygen groups such as epoxides, tertiary alcohols and peripheral carboxylic acids.[10] These strategies have previously been used to attach various molecules ranging from chromophores,[15] antibodies,[16] polymers[17] and nanoparticles.[18]

Modifying the surface of graphene in such a manner introduces defects into the planar graphitic layers that can ultimately serve to diminish the valuable aforementioned properties. An accessible solution to this problem is the exploitation of supramolecular methods towards the development of hybrid graphene nanostructures[19] through the inclusion of biocompatible, flat and aromatic synthons such as NDIs. This can provide the benefit of a facile approach to

modifying graphene surfaces that relies primarily on electrostatic and Van der Waals interactions. Furthermore, such approach eliminates the need for using graphene oxide and covalent methods. Smaller fragments of larger carbon nanostructures can be used to model the supramolecular binding behaviour of larger carbon nanoforms.[20],[21] Thus, smaller nanostructured portions have been previously used to study the association of a fullerene fragment with a chromophore in a host-guest system.[22]

Flat, aromatic and biocompatible, functionalized electron acceptor systems such as NDIs have attracted much attention in recent years, particularly in the design of conducting materials, due to their tendency to form n-type over p-type semiconductor materials.[23] They are capable of self-assembly[24] and intercalating to incorporate themselves into larger multicomponent assemblies.[25] When functionalized with a variety of biocompatible tags, NDIs are versatile synthetic scaffolds and their potential applications are already extending to biomedical imaging fields.[26],[27],[28],[29] These aromatic molecules have demonstrated their capability to across cellular membranes[30],[31] and favour the up-take of carbon based materials such as Single Walled Carbon Nanotubes (SWNTs).[32] Such behaviour seems to be independent from the primary amine employed for the synthesis of NDIs and rather be driven by the planar naphthalene diimide cores.[30],[31],[32] The phenylalanine tagged NDIs demonstrate reasonable 2-photon cross-section areas[33] and despite their rather low quantum yields, can be successfully used as imaging probes in prostate cancer cell due to their broad fluorescent emission.[30] These optical properties combined with biocompatibility have rendered them ideal candidates for further functionalization and exploitation for fluorescent bioimaging.[29, 30, 32]

The assembly process between NDIs and nanomaterials such as C_{60}, C_{70} and SWNTs has been explored, by us and others.[32],[34],[35],[36] Recently, an interest in understanding their interactions with planar carbon systems (denoted here PCS) has emerged and these are believed to be based on non-covalent contacts such as π-stacking coupled with hydrophobic

interactions and Coulombic attractions of the electron deficient NDI core to the electron rich surface of graphene and its derivatives.[37] Zhang *et al.*[38] demonstrated the ability of NDIs to interact with allotropes of carbon on a supramolecular level by showing the improved dispersion stability of graphene in water when complexed with N,N'-bis-[2-(ethanoic acid sodium)]-NDI after exfoliation of sheets of graphene by sonication. The authors attributed this improved dispersion stability to the formation of a ground state π-π stacking interaction of the naphthalene core of the NDI and the extended π-system of graphene. Charge transfer interaction within hybrid nanostructures were also recently investigated by assembling amphiphilic NDIs and coronene derivatives leading to 1D nanofibers.[39] Recently fluorogenic composite materials (FCM) have been developed by assembling a dye with a quenching material such as graphene, TRGO, and gold nanoparticles.[40] Fluorescent molecules can spontaneously assemble onto the surface materials due to positive supramolecular interactions and generate Föster Resonance Energy Transfer (FRET) mechanism that may result in a stable photoexcited complex. One of the characteristics of the FCM formation is a general quenching of the dye fluorescence and its quantum yield. This is due to the FRET effect between the dye (FRET donor) and the carbon-based material (FRET acceptor). Carbon-based materials, especially carbon nanotubes (CNTs) and graphene oxide (GO), have recently been explored as FRET acceptors while inorganic or organic dye are used as donor. [40, 41],[42],[43],
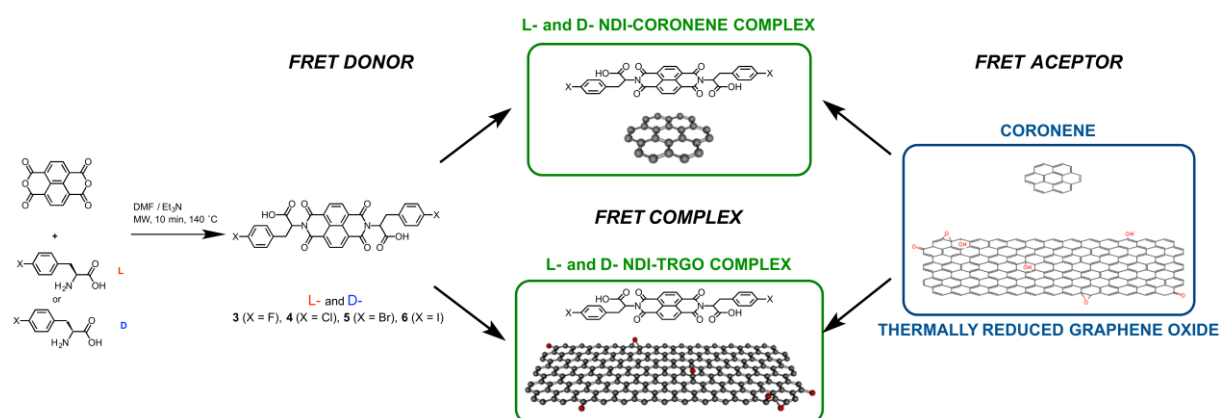
Scheme 1. Schematic representation of the formation of the NDI – planar carbon system complex.

Herein, we report the synthesis and full structural, optical and electrochemical characterization of an entirely new series of α-amino acid functionalised naphthalenediimide. We demonstrate that this class of functional NDIs acting as a FRET donor and incorporating derivatives of phenylalanine can be used to effectively bind and solubilise the planar aromatic 7-ring fused system of coronene as well as thermally reduced graphene oxide (TRGO) (FRET acceptor) (**Scheme 1**). Binding constants and associated kinetic parameters for the host-guest complexes have been calculated via NMR and UV-Vis absorptions in the solution phase. Fluorescence spectroscopy, TCSPC were investigated to describe FRET mechanism indicating the presence of a charge transfer interaction. Cyclic voltammetry studies were carried out to study the redox behaviours of such NDIs and to shed light on the hypothesis that their LUMO energies satisfy the electronic conditions for charge transfer. The use of coronene as a small-molecule model for graphene nano-sheet provides a platform with a defined structure and molecular weight that allows for more systematic studies into the kinetics and thermodynamics of the supramolecular association between chromophores and reduced graphene oxide. This allows, for the first time, a detailed understanding of the strength of such interactions in the solution or the dispersed phase and the reliable study of the resulting NDI-TRGO nanohybrid both in the solid state and in the dispersed phase. We have also investigated the potential of such complexes in biological applications demonstrating the conditions for a strong quencher such as TRGO to be successfully used for in vitro bioimaging purposes. Moreover, the functionalization of TRGO and coronene with NDIs remarkably reduces cellular toxicity and opens up new possibilities to use graphene-like materials for biological applications.

2. Results and discussion

A series of four NDI derivatives was synthesized via a microwave assisted reaction of naphthalenetetracarboxylic acid dianhydride (NDA) **1** with 4-X-D-phenylalanine (X = F, Cl, Br, I, **Scheme 1**), which allows the laboratory scale isolation of such materials with an almost quantitative yield under conditions amenable for sustainable chemistry applications and scale-up, [44],[45] using microwave heating (140 °C for 10 minutes).

It is known that peptide drugs made up of L-amino acids and designed for biological applications typically have poor absorption, distribution, metabolism, and excretion (ADME) properties with sometimes low permeability and low stability.[46] One of the strategies employed for stabilizing peptide derivatives is replacing L-amino acids with D-amino acids.[46],[47],[48] Therefore, we have designed our NDI series using non-natural D-phenylalanine derivatives. We have also carried out cellular toxicity tests on both L- and D-NDI series to compare and assess the effect of the amino acid configuration on cellular viability (for details vide infra and ESI).

Compounds D-**3**, D-**4**, D-**5** and D-**6** were fully characterized by mass spectroscopy, 1D and 2D multinuclear ^{1}H, ^{19}F and ^{13}C NMR spectroscopy, UV-Vis and fluorescence spectroscopy (ESI). NMR spectra and associated assignment data are reported in the ESI. ^{1}H NMR revealed a first order spin system $A_4I_2I'_2MXX'$ in agreement with the functionalization of naphthalenetetracarboxylic dianhydride **1** with 2 equivalent of **2** resulting in a symmetric di-substituted NDI structure. This has been also confirmed by single crystal X-ray diffraction analysis of the derivative D-**3** (vide infra). Compounds D-**3**, D-**4**, D-**5** and D-**6** were obtained in pure form after a simple workup (see Experimental Section) and no further purification steps were necessary. UV-Vis spectra of the series of NDIs show three absorption bands at 330, 350 and 370 nm with a maximum absorbance in the latter. The relationship between absorbance and NDI concentration was investigated in THF with different NDI concentrations, ranging between 0.005 and 0.05 mM to calculate the molar extinction coefficient (ε_{max}).

7

Table 1. Molar extinctions and Quantum yields of NDIs. Values of ε_{max} are reported for comparison in table 1 together with quantum yield (ϕ).

NDI	Molar Extinction Coefficient, ε_{max} (L mol^{-1} cm^{-1})	Quantum Yield, ϕ
D-**3**	2.15×10^4	0.014
D-**4**	1.03×10^4	0.012
D-**5**	1.74×10^4	0.019
D-**6**	1.15×10^4	0.021

X-ray diffraction analysis of p-fluoro-(denoted L-**3**·C_6F_6), (D-**3**), was performed on a suitable single-crystal and reveals structural information on the spatial structures for these amino acid tagged compounds. The intrinsic nature of the planarity of the naphthyl core of D-**3**, D-**4**, D-**5** and D-**6** is a key aspect to rationalise any possibility that in spatial terms, an eventual host-guest interaction between NDIs and coronene may occur. Single crystals of compound D-**3** suitable for X-ray diffraction analysis were obtained from two different saturated solutions of D-**3** in chloroform filtered through a PTFE membrane (denoted D-**3**·CHCl$_3$). NDI solutions were then stored at −20°C or room temperature overnight to allow crystal growth. In both cases the same structure was obtained. A stereoisomer of D-**3** were also obtained from a solution of L-**3** in hexafluorobenzene and (denoted L-**3**·C_6F_6). For simplicity, here, we report the structure of compound D-**3**·CHCl$_3$, as both structures show a similar NDI skeleton (ESI Table S1, S2 and S3). However, more details about the structure of L- **3**·C_6F_6 can be found in the ESI together with the Xray crystal structure of the nonsubstituted L-phenylalanine-NDI (L-**7**) obtained in N-Methyl-2-pyrrolidone (NMP) and denoted (L-**7**·NMP).
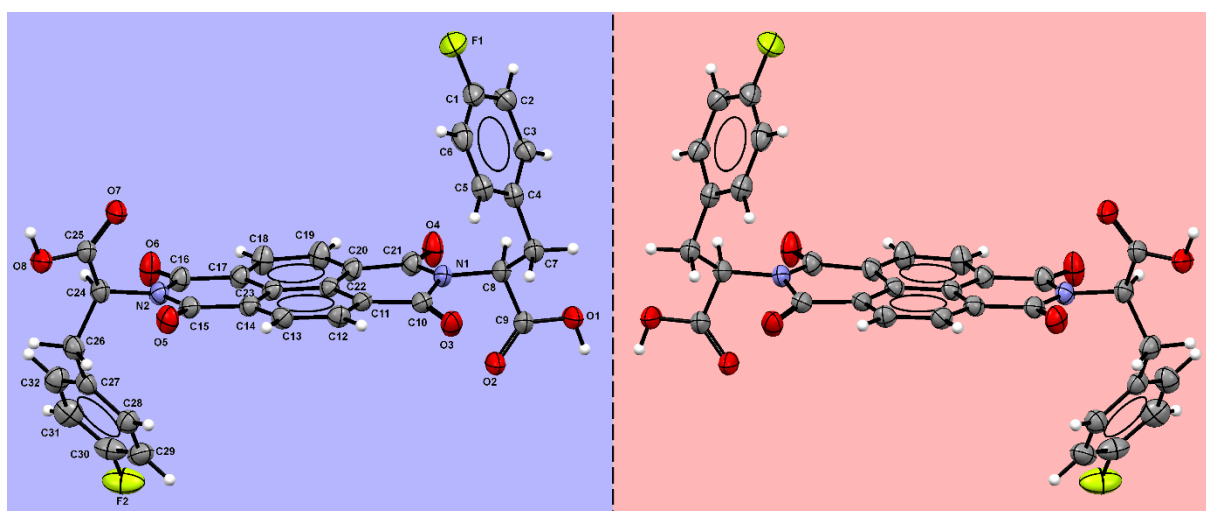
Figure 1. Molecular structure of D-**3**·CHCl₃ (blue background). Thermal ellipsoids at 50% probability. On the right, representation of L-**3** (red background).

The structure of compound D-**3**·CHCl₃ is displayed in **Figure 1**. Structural data, selected bond lengths and angles and hydrogen bond tables are provided in the Supplementary Information (Table S1, S2 and S3).
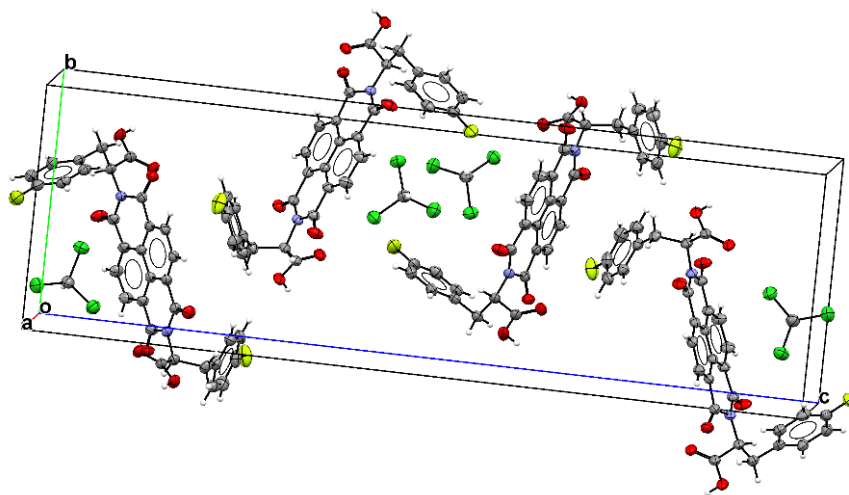
Figure 2. Molecular structure of D-**3**·CHCl₃ showing the unit cell. Thermal ellipsoids at 50% probability. The red, green, purple, grey, white and yellow colored atoms represent O, Cl, N, C, H and F, respectively.

Compound D-**3**·CHCl₃ crystallizes in the orthorhombic space group P2₁2₁2₁, with four symmetrically equivalent NDI molecules and solvent molecules in the unit cell (**Figure 2**). The tilt angles between fluoro-phenylalanine moieties and longitudinal direction of the NDI

skeleton are 73.5° (**Figure 3**). Interestingly, the naphthyl core is not planar, with the N1, C10, O3, C21, O4 atoms lying 7.1(2)° and N2, C15, O5, C16, O6 atoms lying 2.3(2)° outside of the mean plane comprised of atoms

Figure 3. Tilt angle comprising of the mean plane of C11-C23 and the axis of fluoro-phenylalanine moiety for D-**3**·CHCl$_3$
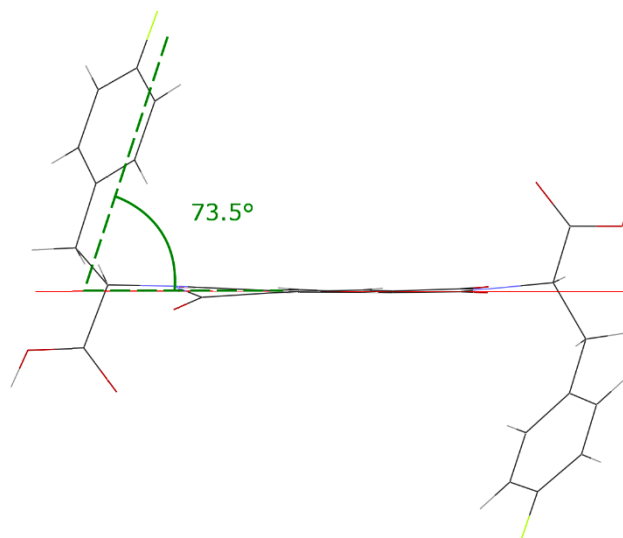
C11, C12, C13, C14, C17, C18, C19, C20, C22 and C23. The two fluorophenylalanine moieties are on opposite sides with respect to the mean plane. The torsion angles of the fluorophenyl groups with respect to the mean plane C11-C23 are 124.1(2)° (the phenyl ring containing the C4) and 78.6(2)° (the phenyl ring containing the C27). Finally, the existence of hydrogen bonds, between the carboxylic groups of neighbouring NDIs, result in an extended H-bonded plane of NDIs (**Figure 4**). The planes are linked together through double short contact interactions between the NDIs, resulting in the stacking of two layers, with two solvent (CHCl$_3$) molecules in the cavity. These arrangements are packed in a herringbone motif (Figure 4). Choice of solvent can play a significant role in the structural arrangement of supramolecular assemblies, thermodynamics of their interaction and their capacity to facilitate charge/energy transfer.[49, 50] Despite the herringbone structure observed in the crystal structure obtained from chloroform, there is the suggestion of a larger extensive hydrogen

10

bonded supramolecular assembly in solutions with minimal to no polarity. The formation of a supramolecular self-assembly of NDIs,
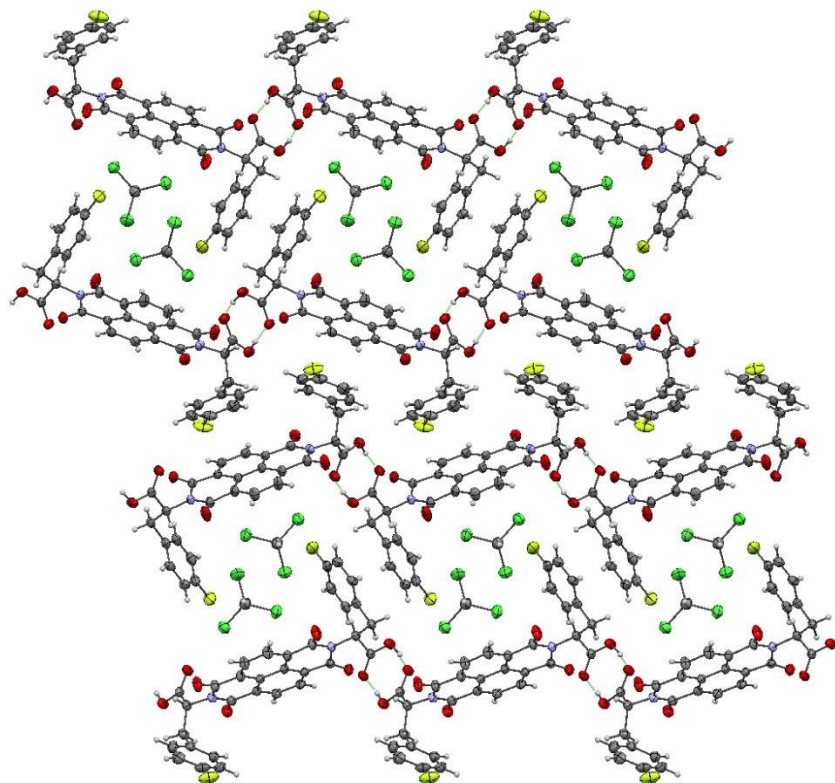

Figure 4. View along the a-axis. Crystal packing structure of D-**3**·CHCl$_3$ displaying the existing hydrogen bonds between the carboxylic groups of neighbouring NDIs. The red, green, purple, grey, white and yellow colored atoms represent O, Cl, N, C, H and F, respectively.

different from that observed in solid state, can be studied by circular dichroism (CD) measurements in solution.[35] Previous studies[51] have shown that NDIs containing aromatic side-groups can lead to the formation of nanotubular structures.[52] However, the choice of solvent can play a significant role in the structural arrangement of supramolecular building blocks.[50] To investigate the nature of the self-assemble of NDIs in solution, the effect of solvent polarity and the size of aromatic complexing agent, CD experiments were carried out in CHCl$_3$ and THF in the presence and in the absence of a FRET acceptor such as coronene and TRGO. The CD spectra of compound L-**3** is shown in **Figure 5**.
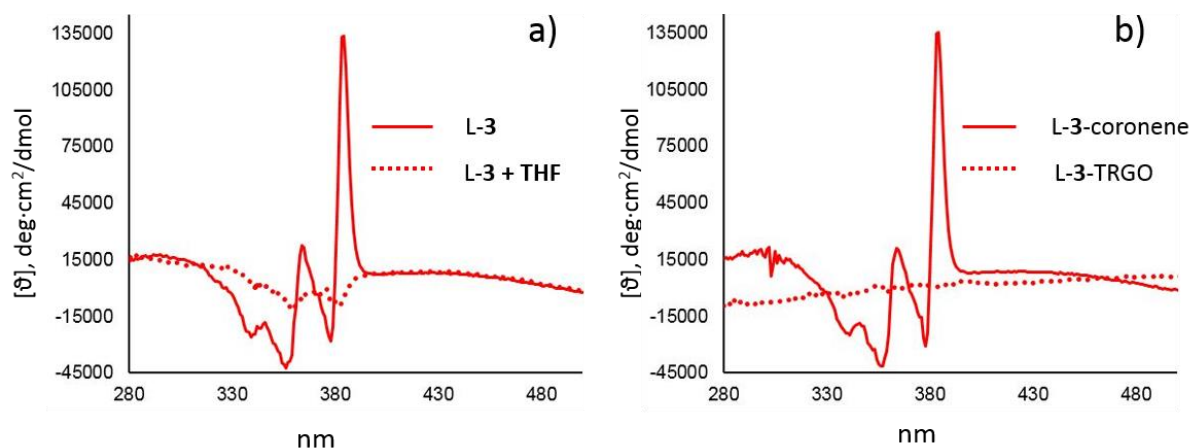
Figure 5 a) CD spectra of compound L-**3** in chloroform (1mM) before (solid line) and after (dotted line) the addition of 20 µL of tetrahydrofuran showing the destruction of the self-assembled nanotubular aggregate upon THF addition.[43] b) CD spectra of compound L-**3** in chloroform (1mM) after complexation with coronene (solid line) and TRGO (dotted line).

The characteristic shape of the CD trace is consistent with a nanotubular assembly that give rise to an induced Cotton effect in a chloroform solvent stabilized with amylene as opposed to ethanol.[53] After the addition of 20 µL of THF, the Cotton effect disappears (**Figure 5a**). This suggests a breakdown of the helical assembly. Therefore, there is a clear indication that any slight degree of polarity in the surrounding molecular environment leads to a set of conditions in which higher order helical aggregate assemblies are highly unlikely. What it is interesting to note is that the signature region of the CD spectrum characteristic of the nanotube is retained in the NDIs·coronene complexes but not in more extended planar congeners such as NDIs·TRGO complexes discussed below (**Figure 5b**). The majority of the studies presented in this work (NMR, UV-Vis, Fluorescence and TCSPC) have been performed in a mixture of THF and toluene. The polarity of the solvents makes it highly unlikely that such a helical arrangement would exist in solution. But it is still interesting to observe such marked differences in supramolecular assembly depending on solvent and size of aromatic complexing agent. CD spectra of L- and D-phenyl alanine NDIs in THF in the presence and

absence of TRGO or coronene are reported in the ESI for comparison (Figure S4-S6). **Figure 6** shows CD spectra of D-**3**, D-**3**·coronene and D-**3**·TRGO complexes and their characteristic CD signatures of π-stacked aggregate .
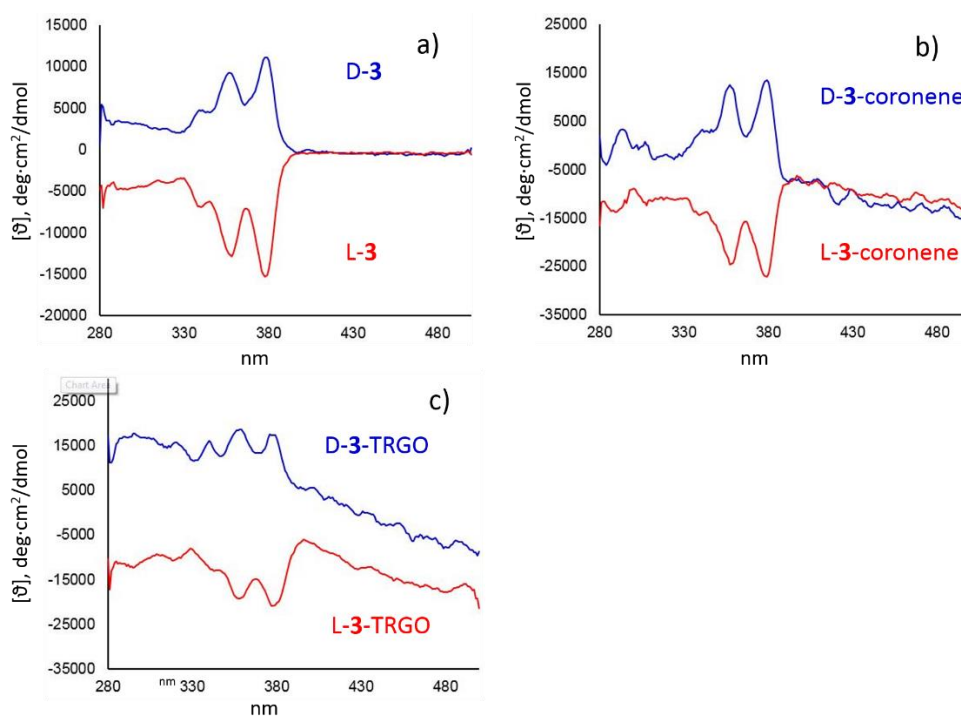

Figure 6. CD spectra of compound L- and D-**3** 0.05 mM in THF (a), L- and D-**3**·coronene 0.05 mM in THF : toluene 1 : 9 (b), L- and D-**3**·TRGO 0.05 mM in THF : toluene 1 : 9 (c).

The elucidation of the electrochemical properties of NDIs has been reported in a number of previous studies, whereby distinct monoelectronic reduction features are observed.[54],[55] Furthermore, electrochemically stable NDIs possessing low-lying LUMO levels have been reported as efficient electron transporting materials.[56] Cyclic voltammetry (CV) experiments were carried out in order to investigate the electron-accepting nature of NDI species and to calculate their associated LUMO energy levels. A standard three electrode system comprising a platinum working electrode, a Ag/AgCl (in solution of KCl) reference electrode and platinum wire counter electrode and the ferrocene/ferrocenium (Fc/Fc+) redox couple as the internal standard was used. General procedures used in the CV experiments are reported in the Experimental section. The voltammograms of each NDI (**Figure 7**) revealed two one-electron

processes which can be associated with the sequential reduction of the two imide substituents, firstly to the anion and then to the dianion species. The redox potential at around 0.5 V is due to the ferrocene redox couple.
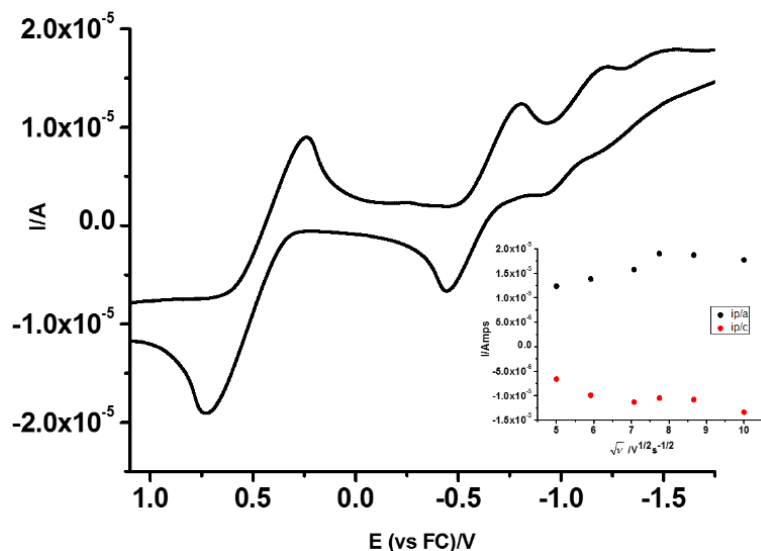

Figure 7. Cyclic voltammogram of D-**3** in THF (5 mM, with ferrocene as an internal standard) at 35 mv/s scan rate. Inset shows peak cathodic and anodic currents dependence with square root of scan rate.

The LUMO energy levels of the six NDI species were determined using the following equation.

$$E_{(LUMO)} = \left[\left(E \quad - E_{\frac{1}{2}ferrocene} \right) + 4.8 \right] (1)$$

Where E_{red} is the voltage at onset of reduction and $E_{1/2\ ferrocene}$ is the half potential of the ferrocene redox couple. The calculated low lying LUMO energies shown below in Table 2 confirm the electron accepting nature of these NDIs and substantiate their potential for the use as host component in a charge transfer supramolecular complex. Half potentials, onset of reduction voltages and LUMO energies of the D-**3**, D-**4**, D-**5** and D-**6** NDIs are reported in Table 2 for comparison.

Table 2. Half-wave, reduction potential and corresponding LUMO levels for NDIs.

NDI	$E_{1/2}$ (V)	E_{red} (V)	E_{LUMO} (eV)
D-3	- 0.62	- 0.53	- 3.78
D-4	- 0.52	- 0.52	- 3.71

D-5	- 0.51	- 0.34	- 3.92
D-6	- 0.55	- 0.52	- 3.74

Novel carbon based hybrid nanosystems were achieved by treating D-**3**, D-**4**, D-**5** and D-**6** NDI molecules with planar carbon systems such as coronene and TRGO. The formation of supramolecular architectures of NDIs and planar carbon system is driven by solvophobic effects. However, the nature of their electron density can play an important role in the self-assembly of NDI and planar carbon systems and facilitate a donor-acceptor charge transfer interfaces. [57] NDIs in this family, including D-**3**, D-**4**, D-**5** and D-**6** molecules contain strongly electron withdrawing groups in the periphery of the naphthalyn core and are suitable for face-centred stacking interactions with electron rich molecules. On the other hand, the π-electron density of molecules such as benzene or its larger congeners (graphene, TRGO, coronene) dominate the area above and below the plane of the hydrogens. By following this approach, we designed and achieved a supramolecular system with electron-rich (*coronene*) and electron-deficient (*NDIs*) building blocks. NMR techniques have been used to calculate the degree of association (K_{ass}) between the host-guest components of the complex NDI_{Gr}·coronene.
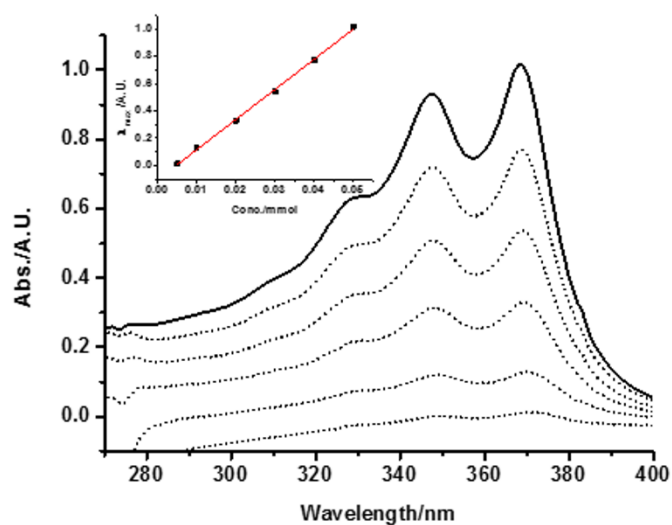
Figure 8. Absorbance spectrum of compound D-**3** at various dilutions: 50 µM (solid line) and subsequently (dotted lines): 40 µM, 30 µM, 20 µM, 10 µM and 5 µM (including the calibration curve) in tetrahydrofuran.

We propose that the assembly between NDI and graphene-like nanomaterials occurs in the first instance via a spontaneous ground state NDI (NDI_{Gr}) interaction with the pi-aromatic system. We also explore the occurrence of a photoinduced energy charge transfer process within the NDI_{Ex}·PCS supramolecular complex. Fluorescence titration experiments were also used to distinguish a photo induced FRET mediated binding mechanism. While TCSPC experiments explore the exponential decay characteristics of the donor acceptor system complexes. **Figure 9** shows the UV-Vis spectra of traces of the coronene (blue line), D-**3** NDI (purple line) and the complex of the two (NDI_{Gr}·coronene, red line). The enhanced solubilisation of coronene is supported by the increased absorbance at 304 and 342 nm in UV region of spectrum. Subtracting the NDI absorbance from that of the complex allows us to visualise the contribution of coronene to the complex which is identifiable by broadening of the shoulder between 290 and 304 nm and is caused by additional sharp peak at 294 nm (green line in Figure 8). The inset of Figure 8 shows the presence of new charge transfer bands not seen in either of the independent host and guest solutions. The appearance of low energy bands at 485 nm arises as a result of electronic transitions between the HOMO of the donor and the LUMO of the acceptor.[58] These transitions were present after increasing the concentration of the host molecule to 1 mM in order to overcome the relatively poor extinction co-efficient of the complex and the low association constant. The choice of solvent for these studies was restricted due to solubility issues. Coronene is known to be only sparingly soluble in THF and was therefore seen as an ideal candidate to verify here its solubility enhancement in the presence of the NDI compound D-**3**.
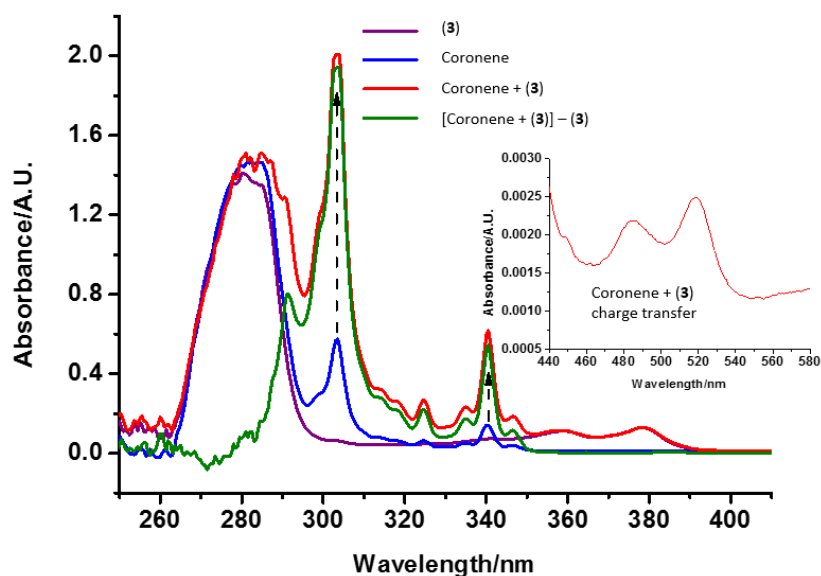
Figure 9. UV-Vis spectra of D-**3** (purple line), coronene (blue line), D-**3**·coronene complex (red line) and. solubility enhancement of coronene system and corresponding charge transfer band in the presence of D-**3** in tetrahydrofuran . The inset shows the presence of new charge transfer bands not seen in either of D-**3** and coronene solutions.

NMR titrations were carried out to approximate the aromatic stacking of graphene-like materials to that of coronene used as a model molecule. In agreement with what has been conventionally reported in the past,[59] the host concentration is the one that is kept constant while being titrated with the guest. In a ^{1}H NMR titration, coronene ('guest' molecule) is gradually added to the NDI ('host' system) solutions and selected ^{1}H chemical resonances are monitored. Considering that supramolecular binding is largely dependent on electrostatic effects, polar solvents such as THF can serve to disrupt the binding due to donation of electron pairs or the acceptance of hydrogen bonds from the NDI units. In order to overcome solubility

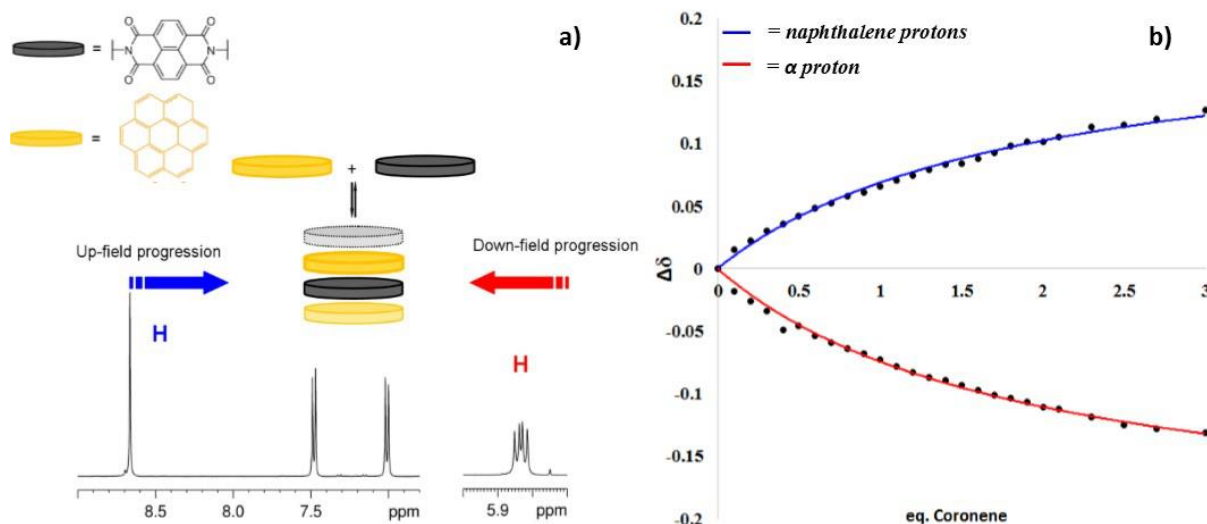**Figure 10. a)** Schematic representation of up- and down-field chemical shifting during a phenylalanine-NDI – coronene ¹H NMR titration. For simplicity we represented only the face centre stacking between coronene and naphthalene core. **b)** Experimental data (markers) and fitting curve (blue and red lines) of a 1 : 1 isotherm binding model at the relative D-**3** : coronene ratio.

issues for the NMR studies, the solvent of choice was mixture of THF-d_8 and toluene-d_8. The inclusion of this non-polar solvent served to enhance the solubility of coronene to the intended titration extent. The use of deuterated THF and toluene also aid in the reduction of solvent-host binding interactions which have been shown to dramatically reduce binding associations by factors of up to 100.[60] For studying the interactions of an electron-deficient electron-rich (or Host-Guest (HG)) complex, the simplest stoichiometries are 1:1, 1:2 and 2:1. It is reasonable to assume that in the presence of a suitable excess of either Host or Guest in solution, binding systems of higher order than 1:1 will form as the structural nature of either Host or Guest can facilitate this.[61]

Jabbari-Farouji and van der Schoot[61] reported a model that described the different possible arrangements of two species conforming to an intricate set of self-assembled ordering systems. For the purposes of simplicity in assessing the influence of the halogen series, we have restricted the discussion to the association constant to the 1:1 complexes. However, we

18

attempted to model the titration data according to 1:2 and 2:1 systems. Full details of higher order stoichiometry models are reported in the ESI.

Table 3. Binding constant $K_a^{1:1}$ is in M^{-1}. Standard error of estimated data (SE™) and convariance of fit (Cov$_{fit}$) are reported and calculated according reference [36].

	1 : 1 (H:G)		
NDI	$K_a^{1:1}$	**SEδ**	**Cov$_{fit}$**
D-3	240	0.002	0.001
D-4	260	0.002	0.001
D-5	550	0.003	0.001
D-6	1730	0.007	0.005

In a typical ^{1}H NMR titration experiment, aliquots of guest (coronene) were gradually added to solutions of D-**3**, D-**4**, D-**5** and D-**6** (THF-d_8 : toluene-d_8 1:9 solution 2.21 mM) as described in the experimental section. The addition of coronene causes an increase of the up-field shifts of the naphthalene protons (blue in **Figure 10**), while the chemical shifts of the alpha proton (red) are deshielded as the titration progresses. For the halogen series of NDI studied, a total of three equivalent of coronene were progressively added during each experiment. The $\Delta\delta$ data were then extrapolated to constitute a data collection that were analysed by Matlab$^\rightarrow$ m-files[59] and then fitted to 1:1 binding isotherm affording values of association constants. A typical up- and down-field progression of the chemical resonances of the naphthalene core (blue) and alpha proton resonances of the phenylalanine moieties (red) of the NDIs, respectively on the relative host-guest ratio, is reported in Figure 8. In Figure 8b, the equivalent of guest added upon titration is plotted versus $\otimes$™ described in the equation (2).

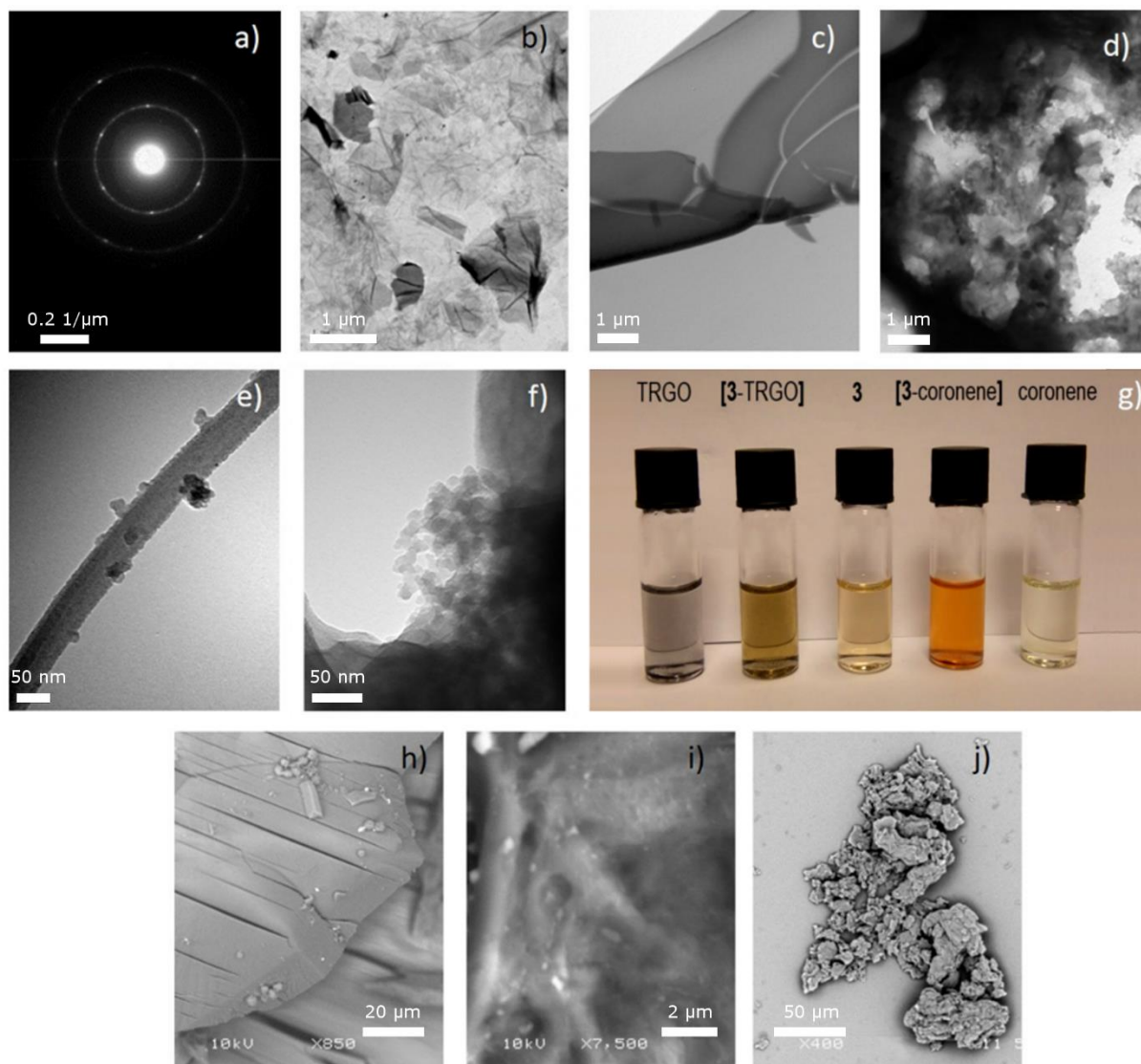$$\Delta\delta = \delta_0 - \delta_{Complex} \quad (2)$$

Figure 11. a) SAED of graphene oxide. b) TEM micrograph of graphene oxide (Scale bar: 1 ⌈m). c) and d) TEM micrograph of D-**3**·TRGO complex (scale bars: 1⌈m). e) and f) TEM micrograph of D-**3**·coronene complex (scale bars: 50 nm). g) from the left to the right: TRGO, D-**3**·TRGO (suspensions in toluene), THF solutions of D-**3**, D-**3**·coronene complex and coronene (toluene) (right). h) SEM micrograph of a single crystal of D-**3** (scale bars: 20 ⌈m). SEM micrograph of D-**3**·coronene complex (scale bars: 2 ⌈m). j) SEM micrograph of D-**3**·TRGO complex (scale bars: 50 ⌈m).

The formation of a 1:1 NDIs$_{Gr}$: coronene complex was indicated by the Jobs plot analysis (ESI).

Other host-guest complexes involving NDI cores in a 1 : 1 ratio with other (unrelated) donor systems have been previously reported.[62] Values of K$_a^{1:1}$ were found to range 13 to 110 M^{-1} for system involving NDI and Zn(II)metallated porphyrins. K$_a^{1:1}$ of phenylalanine tagged NDIs D-**3**, D-**4**, D-**5** and D-**6** reported in table 3 are up to three orders of magnitude higher

20

($K_{a(3)}^{1:1}$ = 1730 M^{-1}) suggesting that coronene is a better guest system for NDIs in a supramolecular assembly in THF - toluene solutions. Comparing the values of $K_a^{1:1}$ of our series, it is interesting to note that a relationship between binding constants, atomic radius and electronegativity of the halogen group exists. The values of $K_a^{1:1}$ follows the halogen trend in which the higher constant is associated with the iodine substituent. These association constants increase from the top to the bottom of the halogen group with $K_{a(3)}^{1:1}$ being approximately one order of magnitude smaller ($K_{a(3)}^{1:1}$ = 240 M^{-1}) than $K_{a(6)}^{1;1}$.

TEM and SEM studies were carried out in order to observe the morphology of NDIs and their adducts with coronene or TRGO. As expected, selected area electron diffraction (SAED) of free TRGO indicates a crystalline structure (**Figure 11a**), while its direct observation by TEM revels a sheet-like material (**Figure 11b**). TEM micrographs of D-**3**·TRGO shows a heterogeneous distribution of the complex with various degrees of aggregation (**Figure 11c** and **11d**). **Figure 11c** shows a well dispersed sheets of D-**3**·TRGO complex, while in a different site of the sample it can be observed a multilayer aggregation structure (**Figure 11d**). EDX analysis of hybrid NDI·TRGO samples confirms the presence of the halogens together with carbon species and, therefore, the formation of the desired NDI complexation (see ESI). The morphology of the D-**3**·coronene complex was also investigated by TEM. A crystalline red powder was obtained by recrystallizing D-**3**·coronene from N-methylpyrrolidone and H$_2$O.[63] The TEM micrographs of D-**3**·coronene shown in **Figure 11e** indicates the formation of crystalline organic nanoparticles of the relevant complex together with amorphous material (**Figure 11f**). The presence of the halogenated complex and carbon species was confirmed by EDX analysis (see ESI). The formation of amorphous D-**3**·coronene complex was also investigated by SEM (**Figure 11i**) together with EDX (see ESI). SEM micrograph of the NDI-TRGO adducts shows a sheet-like surface morphology (**Figure 11j**), while EDX analysis confirm the presence of NDI and TRGO (see ESI). These results indicate that D-**3**, D-**4**, D-**5** and **6** can be complexed by planar carbon system such as coronene and TRGO. When NDIs

are complexed by coronene, the supramolecular assembly can generate organic nanoparticles, while functionalised carbon nanosheets can be observed in NDI-TRGO adducts. However, a certain degree of aggregation of amorphous material can be seen.

The emission properties of NDIs of interest D-**3**, D-**4**, D-**5** and D-**6** can be easily monitored using fluorescence spectroscopy in solution. They are consistent with the expectations for systems that act as sensor candidates because of the tunability of fluorescent properties.[34][64],[65] By exciting compounds D-**3**-D-**6** at λ_{exc} = 380 nm, emission bands were observed in the relevant spectra in the range of 470-670 nm. Fluorescence spectra of D-**3**, D-**4**, D-**5** and D-**6** show a typical emission structure characterised by two strong energetic transitions at *ca*. 530 and 570 nm (**Figure 12, Figure 13** and ESI). The ability of the excited state NDIs (NDIs$_{Ex}$) to interact with carbon based system was further assessed via 2D fluorescence spectroscopy, qualitative fluorescence titration experiments and quenching process.
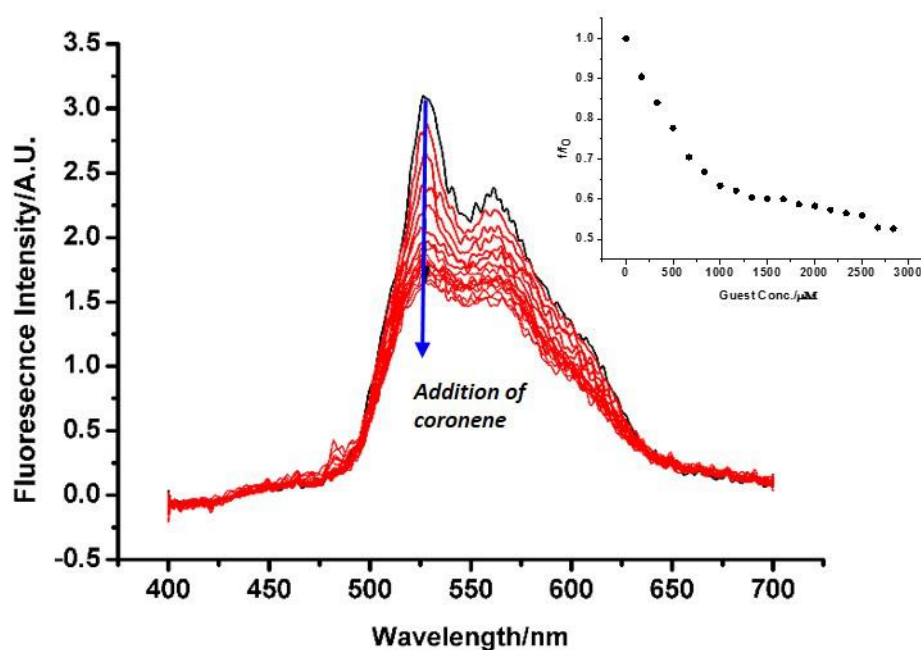

Figure 12. Fluorescence emission quenching in a solution of Compound D-**3** (10 mM) during titration of Coronene (3000 μM) in a 1:1 mixture of Toluene and THF. The inset shows the normalised fluorescence emission intensity at 380 nm excitation at the relevant coronene concentration.

Normalized 2D fluorescence contour plots indicate that such a relevant quenching process occurs in solution and applies to all the species capable of emitting in between 200 - 800 nm including NDIs and quenchers (coronene and TRGO) that are in equilibrium with their corresponding complexes.

Two-dimensional fluorescence contour plots were recorded for free D-**3** and its complexes with coronene and TRGO (Figure 13). Following the complexation of D-**3** by coronene, the strong emission region between *ca*. 530 and 570 nm is attenuated and severally quenched upon TRGO interaction. Fluorescence titrations were carried out on the halogenated series of NDIs (10 mM) with coronene (3000 μM) and TRGO (2 mg/ml) (see section 6 of the ESI). Figure 12 shows how the relevant emission peaks of compound D-**3** were gradually quenched when coronene or TRGO were added (see Figure S31-S37 of the ESI). We propose that within the systems studied quenching occurs via Förster Fluorescence Resonance Energy Transfer processes. General procedures for the fluorescence titrations are reported in the Experimental section. For any transfer to occur then the excited molecule must be photoactive, i.e. they must absorb and emit photons efficiently.
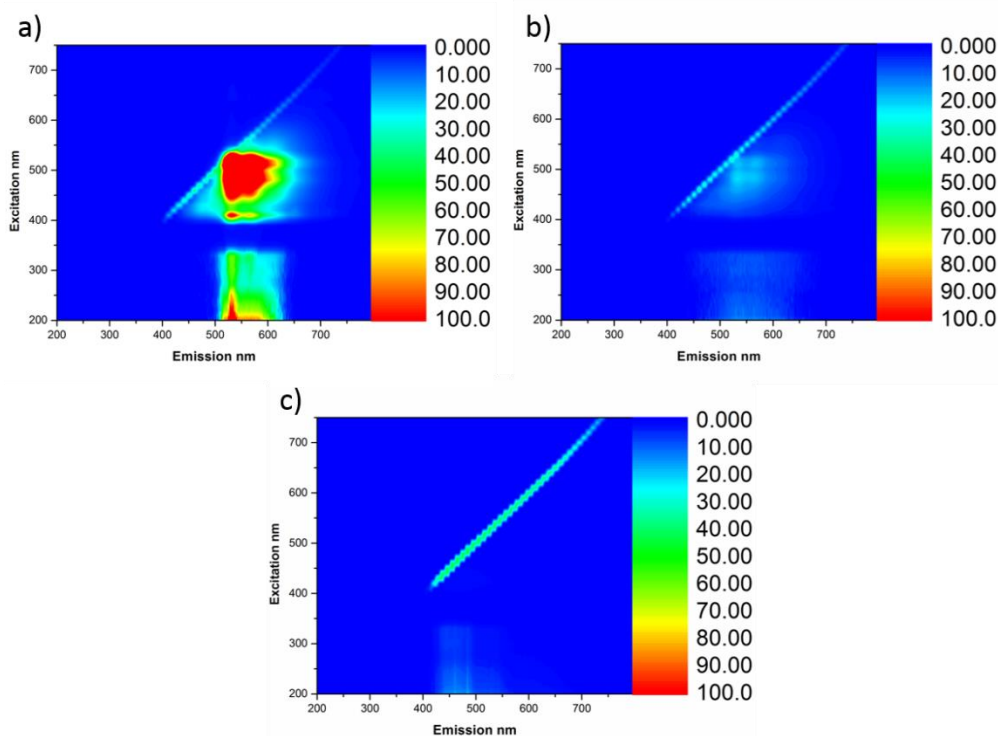
Figure 13. Normalized 2D fluorescence contour plot of a) free D-**3** (10 mM in THF), b) D-**3**·coronene complex (10mM in THF) and c) D-**3**·TRGO (2 mg/ml suspension of TRGO in a solution of D-**3** 10mM in THF) composite showing a relevant quenching process. Details on solution and suspension preparation are reported in the experimental section.

Overlap of the donor emission spectrum and the acceptor absorption spectrum is required, such that energy emitted by the excited donor to the ground state may excite the acceptor species. Indeed both coronene and TRGO exhibit broad absorption characteristics around the emission band of D-**3**, D-**4**, D-**5** and D-**6** molecules and therefore FRET may be facilitated.

Time correlated single photon counting measurements were carried out in order to further investigate the excited state characteristics of NDI$_{Ex}$·coronene and NDI$_{Ex}$·TRGO complexes. **Figure 14** shows the fluorescence lifetime decay of free D-**3**, D-**4**, D-**5** and D-**6** together with their coronene and TRGO complexes. When in free solution, the fluorescence decay of compounds D-**3**, D-**4**, D-**5** and D-**6** could be fitted to a single component system with χ^2 (describing the goodness of the fitting and 1 is optimum) ranging between 1.16 to 1.29 showing single lifetimes of approximately 3.5 - 3.8 ns (**Table 4**). However, two component systems were more accurate models of the decay profiles when either coronene or TRGO was present.
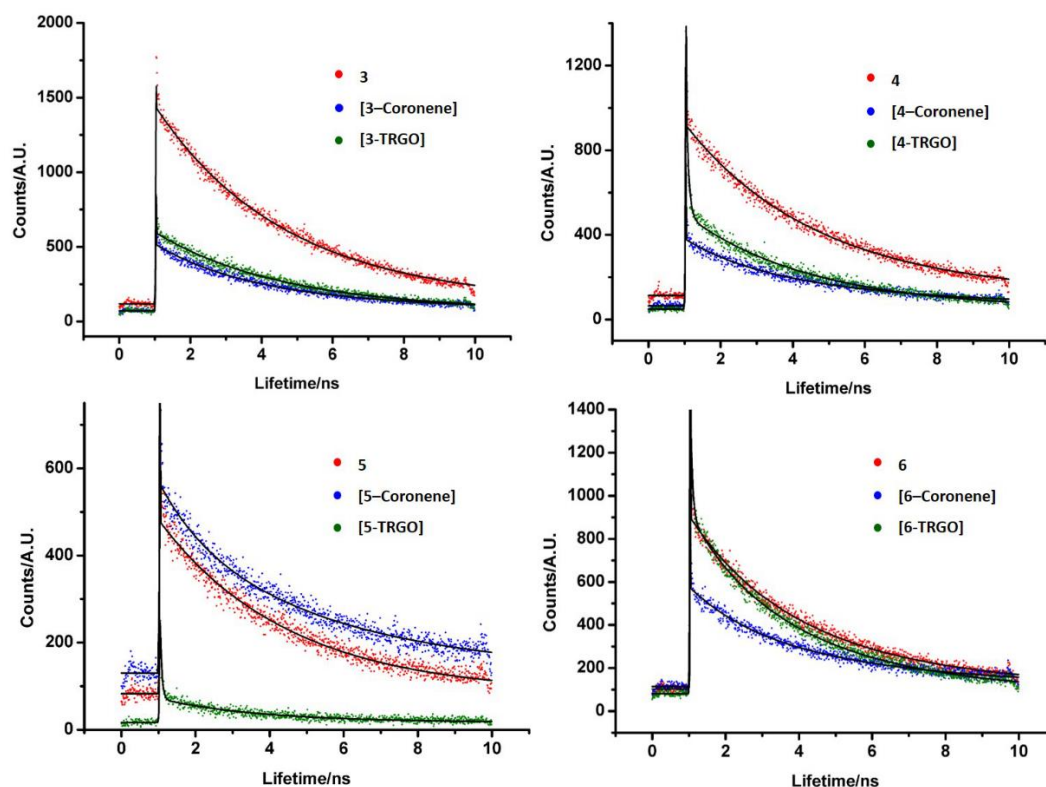
24

Figure 14. Fluorescence lifetime decay traces (λ_{exc} = 810 nm, 5.5 mW) of D-**3**, D-**4**, D-**5** and D-**6** (50   nM solutions in tetrahydrofuran, red), their relative NDI·coronene complexes (50 µM solutions in tetrahydrofuran, blue) and NDI·TRGO complexes (tetrahydrofuran dispersion containing 50 µM of NDI and 2 mg/ml of TRGO, green).

This implies the presence of new emitting species as a result of complexation. All of the NDIs showed single lifetimes of approximately 3.3-3.7 ns when free in solution. Upon complexation however a shorter major lifetime component (τ_1) and a longer minor component (τ_2) were apparent. Interestingly, the major component for the NDI·TRGO complexes was reduced quite dramatically (46 to 329 picoseconds). Therefore, it is reasonable to assume that these changes in lifetime upon complexation, particularly the additional shorter component may account for a photo-induced excited state electron transfer occurring between the closely bound donor-acceptor systems within the NDI$_{Ex}$·TRGO and NDI$_{Ex}$·coronene complexes. Finally, it is worth noting that the τ_1 for the NDI$_{Ex}$·TRGO species was found to be considerably shorter suggesting that TRGO is a more severe quencher than coronene. The appearance of a second longer minor component might suggest the presence of unquenched species free in solution or their supramolecular aggregates.

25

Table 4. TCSPC fluorescence lifetime data for free NDIs (50 µM) and when complexed with coronene (100 µM) or TRGO (saturate and filtered solution) in THF.

	Single Component (ns)	χ^2	Two Component (ns)		χ^2	%	
			τ1 (ns)	τ2 (ns)		a1	a2
D-3	3.75	1.29	-	-	-	-	-
D-3·coronene	-	-	2.24	4.9	1.29	71	29
D-3·TRGO	-	-	0.329	4.16	1.08	73	27
D-4	3.79	1.25	-	-	-	-	-
D-4·coronene	-	-	1.74	4.68	1.18	75	25
D-4·TRGO	-	-	0.069	3.48	1.21	76	24
D-5	3.49	1.16	-	-	-	-	-
D-5·coronene	-	-	1.2	4.66	1.17	69	31
D-5·TRGO	-	-	0.046	3.76	1.15	74	26
D-6	3.49	1.19	-	-	-	-	-
D-6·coronene	-	-	1.53	4.55	1.27	73	27
D-6·TRGO	-	-	0.054	3.70	1.20	70	30

This particular work demonstrates that doping of planar carbon based system can be achieved by using amino acid tagged NDI building blocks. The TCSPC of the NDIs in free solution does not show a multi component exponential decay in these particular experimental conditions. Therefore, this complexation suggests the features of the resulting composite have the potential to be more than the sum of the individual properties of the constituent molecules in a low concentration regime. The TCSPC has also the merit of allowing us to study the emission properties of our systems at concentration far lower (50 µM) than the one used for fluorescence titrations. These experiments assured that the quenching mechanisms emerging from fluorescence titrations and TCSPC reflect the formation of a carbon-based NDI nanohybrid rather than NDI-NDI aggregates.

Laser scanning confocal microscopy has been performed on NDIs, NDI·coronene and NDI·TRGO complexes in order to establish their potential as cancer imaging agents. PC-3 cells were grown according to standard serial passage protocols, plated onto glass bottom

dishes and allowed to grow up to a suitable confluence (see ESI for cell culture and plating details). **Figure 15** shows the bright field image, the emission overlay of the blue-green-red channels, the individual channel emissions (blue: λ_{em} = 460 nm, green: λ_{em} = 525 nm, red: λ_{em} = 629 nm) of compound D-**3** (**Figure 14a-e**), D-**3**·coronene (**Figure 14f-j**) and D-**3**·TRGO (**Figure 14k-o**).
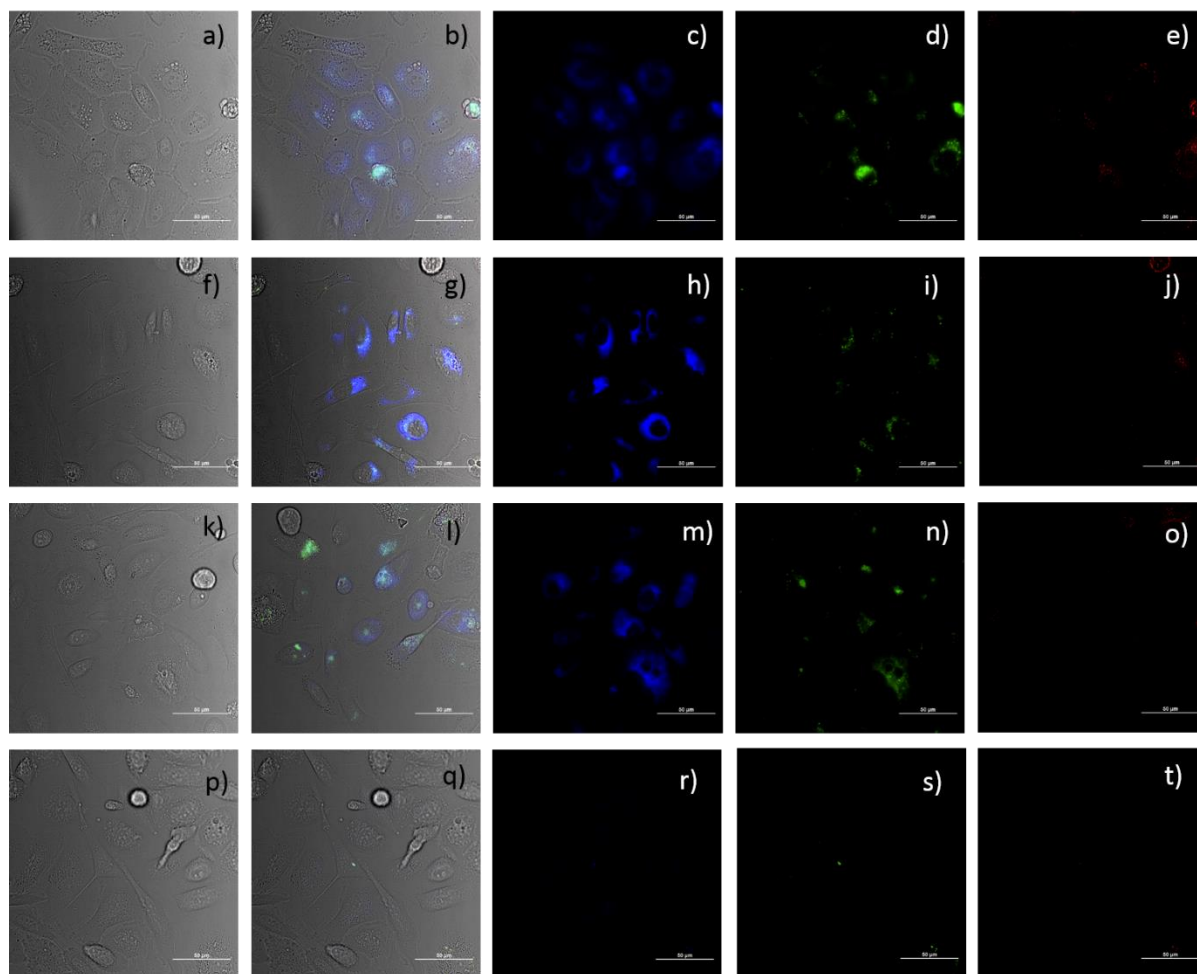

Figure 15 Epi-fluorescence acquisition of PC-3 cells incubated for 15 minutes with compound D-**3** (a-e), D-**3**·coronene (f-j), D-**3**·TRGO (k-0) and DMSO control (p-t). Final concentrations 50 μM in 5 : 95 DMSO : serum free medium at 37 °C. DIC channel (a, f, k, p); overlay of DIC-blue-green-red channels (b, g, l and q); blue channel, λ_{em} = 460.0 nm (c, h, m, r); green channel, λ_{em} = 525.0 nm (d, i, n, s); red channel λ_{em} = 629.5 nm (e, j, o, t). Scalebar: 50 μm.

It is clear that there is up-take of D-**3** and its carbon nanocomposites in PC-3 cells, with the majority of the emission lying within the blue and green wavelengths with some minor emission in the red wavelengths. Considering this success, further images with confocal

settings were taken in order to gather more information regarding cellular uptake and distribution.

Figure 16 shows the images of PC-3 cells incubated for 15 minutes with compound D-**3,** D-**3·**coronene and D-**3·**TRGO taken in the confocal mode with a large majority of the emission lying in the blue and green wavelengths. However, it is much clearer that there is broad emission across all of the visible wavelengths including the red. This is consistent with the fluorescence studies presented earlier in the work whereby the NDIs demonstrated broad emissive characteristics ranging from 400 to 700 nm of the visible spectrum. Similarly to what was seen for compound D-**3**, D-**3·**coronene and suspensions of D-**3·**TRGO can be successfully taken-up in PC-3 cells and, therefore, potentially employed as cancer imaging agents. From the confocal microscopy it seems that the NDIs, NDI·coronene and NDI·TRGO complexes localise throughout the cell cytoplasm. However there seems to be no emission coming from the nuclear regions within the cells
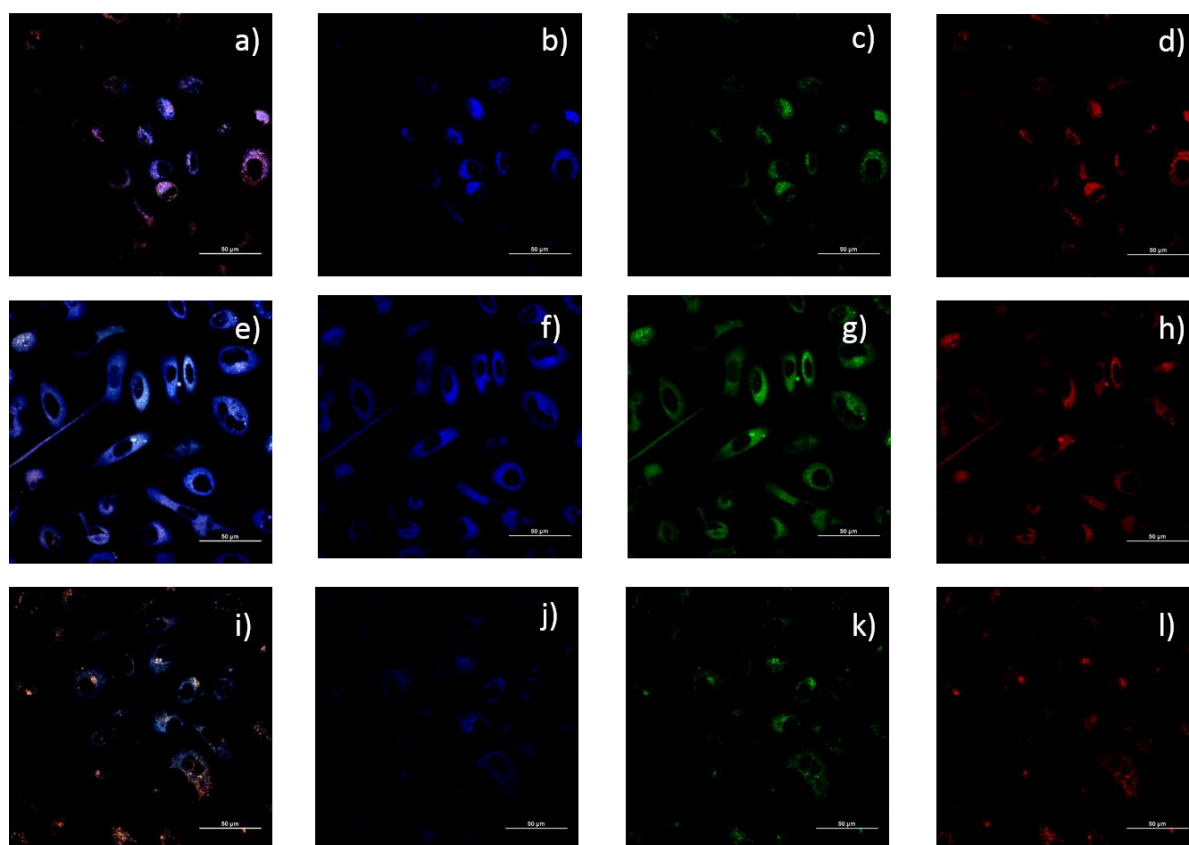
Figure 16. Single-photon laser-scanning confocal microscopy of PC-3 cells incubated at 37 °C for 15 minutes with D-**3** (a-d), D-**3**·coronene (e-h) and D-**3**·TRGO (i-l) (50 μM, in 5 : 95 DMSO : serum free medium). (a, e, i) overlay of the blue-green-red channels, (b, f, j) blue channel (417-477 nm), (c, g, k) green channel (500-550 nm), (d, h, l) red channel (570-750 nm). λ_{ex} = 405.0, 488.0 and 561.0 nm. Scale bar: 50 μM.

suggesting an inability of the NDIs as well as NDI·coronene and NDI·TRGO to penetrate the nuclear membrane. It was therefore deemed necessary to perform depth scans across the entire sample to confirm uniform distribution of the NDIs within the cell cytoplasm. Z-series section scans were performed on the samples in order to generate, from *in-vitro* fluorescence emission, 3D images of PC-3 cells exposed to NDIs, NDI·coronene and NDI·TRGO (Figure S53-S60 of section 10 of ESI). The presence of the outline of the entire cell structure is a clear indication of uniform distribution throughout the cytoplasm. The inability of the naphthalene core to penetrate the nuclear membrane is consistent with what we recently observed for RGD-peptide tagged NDI molecules.[30] Carbon nanostructure such as SWNTs complexed with NDIs seemed to be responsible for a low degree of nuclear membrane penetration.[32] The present data is in agreement with out previous findings, highlighting that the interaction of NDIs and PCS is robust enough to allow the distribution of NDI·coronene and NDI·TRGO complexes in the cytoplasm, by preventing the carbon-based material to cross the nuclear membrane. Although our studies proved that planar carbon systems are responsible for quenching effects on the NDI fluorescence, NDI·coronene and NDI·TRGO nano-hybrids retain the ability to generate suitable fluorescence emission *in vitro*. To verify whether the stability of NDI·TRGO composites remains *in vitro* with respect to NDI loss, two-photon fluorescence lifetime imaging was performed on both of D-**5** and D-**5**·TRGO. The compound was incubated with PC-3 cells at a 100 μM concentration in 1 % DMSO for 15 minutes. **Figure 17** shows the lifetime distribution and exponential decay curves of D-**5** in a free and TRGO complexed state in comparison to the control experiments. The major lifetime components measured in PC-3 were 0.9 ns for free D-**5** and 0.43 ns for D-**5**·TRGO. The presence of a shorter lifetime for the complex suggests that the NDIs undergo quenching of

fluorescence in vitro similar to the solution phase. However, the lifetime profile does not completely overlay with that of the control experiments performed with DMSO. Therefore, the lifetime observed cannot be attributed entirely to autofluorescence or the free NDI. The existence of independent emissive lifetime characteristics and a certain degree of fluorescence quenching indicates that the interaction between the NDI and TRGO is still stable in vitro. The lifetime data are summarised in Table 5.
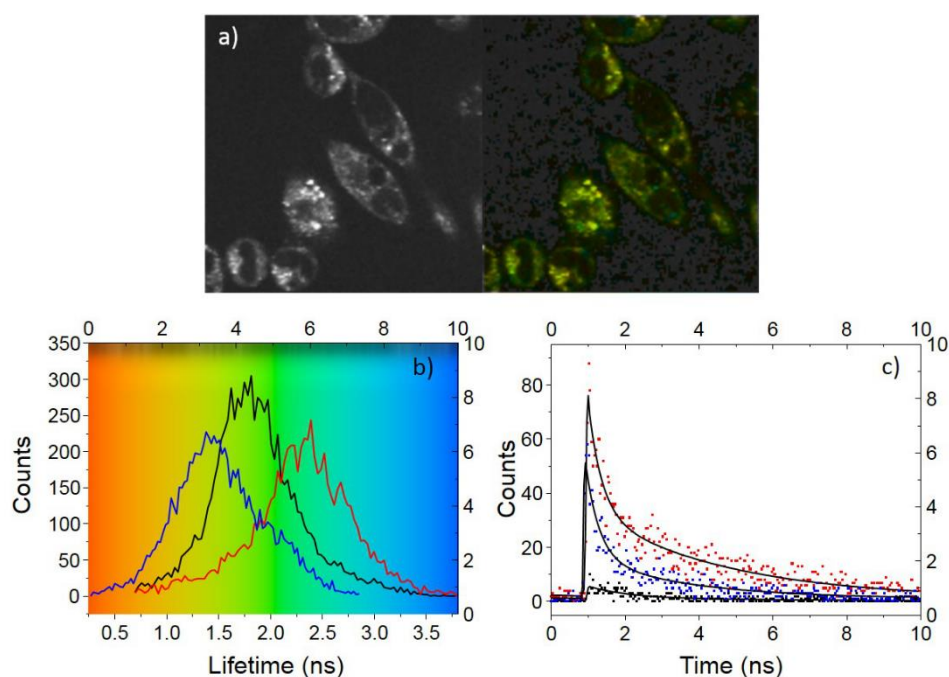

Figure 17 Two-photon fluorescence lifetime map in PC-3 cells of compound D-**5** complexed with TRGO (a) and associated distribution curve comparison of the control and compound D-**5** in free and complexed state (b) and associated lifetime decay profiles (c) at 100 μM after 810 nm laser irradiation.

Table 5. *In vitro* fluorescence lifetime data for free NDIs (10 μM, 1 : 99 DMSO : PBS) and when complexed with coronene or TRGO (saturate and filtered solution).

	Two Component (ns)		χ^2	%	
	τ_1 (ns)	τ_2 (ns)		a_1	a_2
Control	0.28	2.25	1.06	69.9	30.1
D-5	0.9	418	1.07	78.9	21.1
D-5·TRGO	0.43	2.58	1.08	68.7	31.1

Standard MTT assays were performed in order to investigate the effect of the phenyl alanine substituents on the cellular viability with respect to the unsubstituted L- and D-NDI. With the only exception of D-Br and D-Cl derivatives, both the L- and D- series of phenylalanine NDIs show comparable values of IC_{50} in a range of 1.10×10^{-4} M and 4.65×10^{-4} M. Interestingly, chloro-D-phenylalanine NDI, compound **4**, exhibited significant increment of biocompatibility reducing cytotoxicity up to a thousand times comparing to the fluoro-L analogue (**Figure 18**).
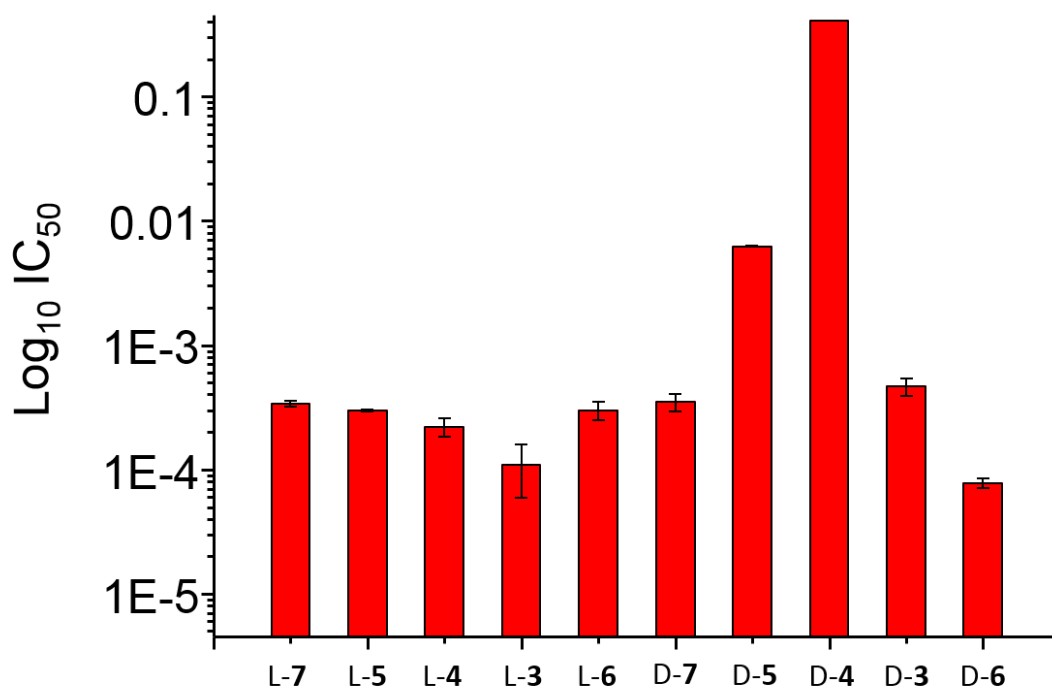

Figure 18. IC_{50} of L- and D-NDI compounds in PC-3 cells over 48 hours incubation at 37 ºC. L-phenylalanine (L-**7**) NDI $IC_{50} = 3.38\times10^{-4} \pm 1.58 \times 10^{-5}$ M; L-**3** $IC_{50} = 1.10\times10^{-4} \pm 5.07 \times 10^{-5}$ M; L-**4** $IC_{50} = 2.22\times10^{-4} \pm 3.73 \times 10^{-5}$ M; L-**5** $IC_{50} = 2.98\times10{-4} \pm 7.92 \times 10^{-6}$ M; L-**6** $IC_{50} = 2.99\times10^{-4} \pm 4.93 \times 10^{-5}$ M; D-phenylalanine (D-**7**) NDI $IC_{50} = 3.47\times10^{-4} \pm 5.66 \times 10^{-5}$ M; D-**3** $IC_{50} = 4.65\times10^{-4} \pm 7.46 \times 10^{-5}$ M; D-**4** $IC_{50} = 0.40 \pm 3.86 \times 10^{-4}$ M; D-**5** $IC_{50} = 6.24\times10^{-3} \pm 5.40 \times 10^{-5}$ M, , D-**6** $IC_{50} = 7.78\times10^{-5} \pm 7.05 \times 10^{-6}$ M.

Therefore, we selected compound D-**4** to investigate how the NDI functionalization of planar carbon systems such as coronene and TRGO affects the cellular viability with respect to free coronene and TRGO. Cell viability in the presence of free coronene, TRGO, D-**4**·coronene and D-**4**·TRGO were, therefore, carried out over a 48 hour observation period. Experimental

details of MTT assays are available in the ESI. Assays showed that the pristine coronene and TRGO had an important effect on the viability of cells showing IC_{50} values of $1.20 \cdot 10^{-5}$ and $2.92 \cdot 10^{-5}$ M respectively. Interesting, the functionalization of TRGO and coronene with D-**4** significantly modulates the biocompatibility of carbon-based materials showing reduced level of toxicity for D-**4**·coronene and D-**4**·TRGO. Remarkably, the IC_{50} values of D-**4**·TRGO is significantly increased, while the viability of cells is enhanced 588 times in the presence of the D-**4**·coronene complex (**Figure 19**). It is known that graphene-family nanomaterials such as graphene, GOs, reduced GOs are cytotoxic and/or genotoxic.[66] Although the mechanisms for their toxicity towards cells are not completely understood as they follow different paths,[67] the formation of reactive oxygen species (ROS) seems to be the most recurring mechanism observed.[68],[69] While pristine carbon based materials tend to accumulate in physiological solution due to electrostatic interactions and nonspecific bindings to proteins,[70] surface modified graphene-like materials are often less toxic.[69],[71] Our results are consistent with these observations. These results demonstrate that the functionalization of coronene and TRGO with D-phenylalanine NDIs considerably improves the *in vitro* biocompatibility of the pristine planar carbon systems presented in this work.

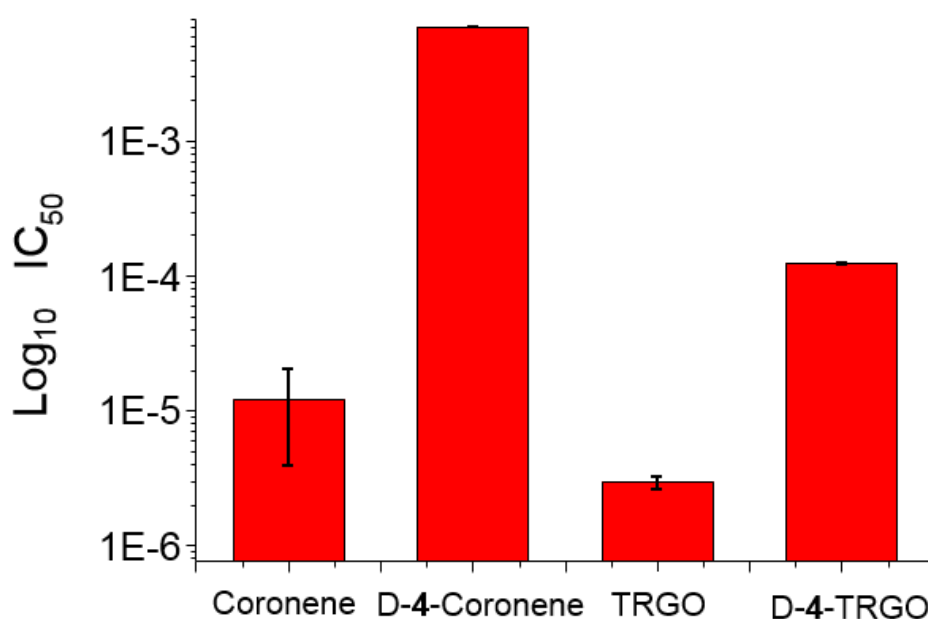**Figure 19.** IC_{50} in PC-3 cells after 48 hours treatment of pristine coronene and TRGO, D-**4**-coronene and D-**4**·TRGO complexes. Coronene $IC_{50} = 1.20 \cdot 10^{-5} \pm 8.17 \cdot 10^{-6}$ M; D-**4**·Coronene $IC_{50} = 7.06 \cdot 10^{-3} \pm 2.03 \cdot 10^{-5}$ M. TRGO $IC_{50} = 2.92 \cdot 10^{-6} \pm 3.05 \cdot 10^{-7}$ mg/mL; D-**4**-TRGO IC_{50} of $= 1.22 \cdot 10^{-4} \pm 2.97 \cdot 10^{-6}$ mg/mL.

3. Conclusion

We evaluated the interactions between halogenated amino-acid tagged fluorescent NDIs and flat aromatic carbon materials. The inclusion of peripheral substituents influences the degree of surface binding to the carbon surface which should be of relevance in the quest of designing tailor made functional nanomaterials. Electron withdrawing organic molecule such as a substituted NDI and electron-rich planar carbon systems such as coronene and their nano-dimensional counterpart thermally reduced graphene oxide both demonstrate the capacity to participate in supramolecular binding processes that are mediated by charge and dynamic excited state energy transitions. Additionally, the size and electronegativity are tunable by the presence of a differing halide substituent at the periphery of the D-phenyl alanine moiety of the NDI allow for a certain degree of control over the surface chemistry of the resulting nanohybrid materials. The inclusion of halogenated species as part of the design opens up opportunities for further manipulation of luminescent properties and tailoring of the materials directionality and strength of the aromatic interaction. These aspects will most certainly prove to be a useful tool in the fabrication of photoactive supramolecular nanomaterials as well as those carbon-based and graphene-like material employed nowadays in biotechnology. *In vitro* fluorescence microscopy carried out on D-phenyl alanine NDIs and their stable coronene and TRGO adducts demonstrates a significant cellular up-take of such carbon-based systems suggesting their potential as prostate cancer bioimaging agents. Remarkably, MTT assays reveal a positive modulation of the biocompatibility for both coronene and TRGO in cellular environment. The results presented in this work show that a deliberate functionalization of the surface of TRGO and graphene-like fragments may lead to a new perspective in the

construction of fluorogenic composite materials, quenching systems and novel FRET-donor-acceptor nanocomposite for biological application.

4. Experimental Section.

4.1 Materials and Method.

All purchased starting materials were used without further purification. All solvents were of reagent grade quality and purchased commercially. Synthesis of compounds D- and L-**3**, **4**, **5** and **6** was carried out under continuous microwave irradiation in a Biotage initiator instrument. Solution multinuclear NMR spectra were recorded on a Bruker Avance 500 spectrometer. ^{1}H and ^{13}C chemical shifts are referenced to tetramethylsilane (TMS). ^{19}F chemical shift is referenced to trichloro-fluoro-methane ($CFCl_3$). ^{1}H and ^{13}C chemical shift assignments were made by using standard COSY (cosygpqf) and HMQC (hmqcgpqf) pulse sequences outlined within the Bruker library. Binding constants were calculated using MATLAB® m files according the procedure outlined by Pall Thordarson.[59]. UV-visible spectra were obtained using a Perkin-Elmer Spectrometer, Lambda 35 in THF and processed using UV Winlab 3 software. Fluorescence spectra were measured in a 1.00 cm quartz cuvette using a Perkin-Elmer LS55 luminescence spectrophotometer. Electrochemical Cyclic Voltammetry analysis was carried out using a standard 3 electrode system comprising a platinum working electrode, a Ag/AgCl (in solution of KCl) reference electrode and platinum wire counter electrode and the ferrocene/ferrocenium (Fc/Fc^{+}) redox couple as the internal standard was used. Two-photon excitation experiments were performed at the Rutherford Appleton Laboratory following the methodology described by Botchway *et al*. 2008.[72] A mode locked Mira titanium sapphire laser (Coherent Lasers Ltd, USA), generating 180 fs pulses at 75 MHz and emitting light at a wavelength of 710-970 nm was used for the 2-photon excitation. The laser was pumped by a solid state continuous wave 532 nm laser (Verdi V18, Coherent Laser Ltd), with the oscillator fundamental output of 915 ± 2 nm or 810 ± 2 nm. The

laser beam was focused to a diffraction limited spot through a water immersion ultraviolet corrected objective (Nikon VC x60, NA1.2) and specimens illuminated at the microscope stage of a modified Nikon TE2000-U with UV transmitting optics. The focused laser spot was raster scanned using an XY galvanometer (GSI Lumonics). Fluorescence emission was collected and passed through a coloured glass (BG39) filter and detected by fast microchannel plate photomultiplier tube used as the detector (R3809-U, Hamamatsu, Japan). These were linked via a Time-Correlated Single Photon Counting (TCSPC) PC module SPC830. Lifetime calculations were obtained using SPCImage analysis software (Becker and Hickl, Germany) or Edinburgh Instruments F900 TCSPC analysis software. Transmission electron microscope (TEM) images were obtained with Gatan Dualvison digital camera on a JEOL 1200EXII transmission electron microscope coupled with Energy-dispersive X-ray spectroscopy (point resolution, 0.16 nm). The samples were deposited on a Cu TEM grid from a THF suspension. Scanning electron microscope (SEM) images were obtained on a JEOL JSM-6480LV scanning electron microscope coupled with an Oxford INCA X-ray analyser. Confocal Microscopy was performed using a Nikon A1Rsi Laser Scanning Confocal Microscope System fitted with 60X oil objective lens, equipped with three lasers (405.0, 488.0 561.0 nm). The microscope was also fitted with a motorized piezo z-stage, halogen lamp and mercury lamp for epi-fluorescence microscopy. All images were processed using functions within the NIS elements software package. 3-dimensional images were generated by a z-stack series of images setting the top and bottom focal planes of the sample. Smoothing function, background subtraction, gauss-laplace filter and matrix expansion were adjusted to interpolate and generate 3-dimensional image of the sample. Circular dichroism spectra were recorded using a Chirascan CD Spectrometer in THF, THF-toluene and $CHCl_3$ stabilized with amylene.

4.2 Synthetic procedures.

1,4,5,8-Naphthalenetetracarboxylic dianhydride (200 mg, 0.746 mmol) and the corresponding α-amino acid derivative (1.491 mmol) were suspended in 5 mL of DMF in a pressure-tight 20 mL microwave vial. To this suspension was added 0.2 mL of dry Et$_3$N. The suspension was sonicated until the mixture became homogeneous. The reaction mixture was heated for 10 min at 140 °C (direct flask temperature measurement) under microwave irradiation using a dedicated microwave system. The solvent was removed under reduced pressure, and each reaction mixture was recrystallized in acetonitrile and 1M HCl yielding the symmetrical NDI derivative product L- and D- **3**, **4**, **5** and **6**. A saturated solution of D-**3** in chloroform was prepared and filtered through PTFE membrane. Solution was stored at − 20°C overnight to allow crystal growth.

4.2 Determination of Molar Extinction Coefficient (ε$_{max}$) by UV/Vis.

Suspensions of D-**3**, D-**4**, D-**5** and D-**6** in chloroform were prepared at a range of concentrations (0.05, 0.04, 0.03, 0.02, 0.01, 0.005 mM). The absorption spectra of these suspensions were then obtained using a Perkin-Elmer Spectrometer, Lambda 35. The maximum absorption of these suspensions at 370 nm was then plotted against concentration and the Molar Extinction Coefficient calculated using the equation A = εcl, where l is equal to path length 0.01 m.

4.3 Determination of Relative Quantum Yield.

Room temperature fluorescence QY was calculated according to the following equation:[73]

$$\phi s = \frac{\frac{\frac{\phi r * Ar}{As} * Es}{Er} * Ir}{Is} * n_s^2}{n_{r^2}} \qquad (3)$$

In this equation subscripts *r* refers to the reference [Ru(bipy)$_3$]Cl$_2$ in water, while *s* is refered to D-**3**, D-**4**, D-**5** and D-**6**. ɸr and ɸs are the fluorescence QY of [Ru(bipy)$_3$]Cl$_2$, (ɸr = 0.042 at 452 in water[74]) and unknown D-**3**, D-**4**, D-**5** and D-**6** respectively. *A* is the absorbance of

the solution, *E* is the corrected emission intensity, *I* is the relative intensity of the exciting light and n is the average refractive index of the solutions.

4.4. Electrochemistry (Cyclic Voltammetry)

The NDIs were dissolved in a 0.1 molar solution of tetrabutylammonium hexafluorophosphate (TBAPF6) in THF to produce a 5 mmol NDI concentration. To these solutions were added equimolar concentrations of ferrocene to act as standard. Samples were purged with Argon before measurements. Experiments were conducted at a range of scan rates between 100 mV s^{-1} and 10 mV s^{-1}. A standard 3 electrode system comprising a platinum working electrode, a Ag/AgCl (in solution of KCl) reference electrode and a platinum wire counter electrode with the ferrocene/ferrocenium (Fc/Fc$^+$) redox couple as the internal standard was used.

4.5. Fluorescence titrations with coronene

A 10 mM solution of NDI was prepared. To this solution was added a saturating quantity of coronene. The resulting saturated suspensions were then sonicated until the mixtures became homogeneous. The excess coronene was allowed to settle. The resulting suspension supernatant was titrated against another 10 mM solution of NDI in THF. Experiments were conducted using a Perkin-Elmer LS55 luminescence spectrophotometer. Excitation wavelength was set at 380 nm for all experiments. Emission range 420-700 nm was scanned at 300 nm min^{-1} for all experiments. Titrations were conducted in a 1.5 mL cuvette. Suspension containing NDI at 10 mM concentration in THF was added to the cuvette and the emission spectrum scanned. Subsequent scans were conducted with 0.2 mL titres removed from cuvette and replaced with 0.2 mL titres of 10 mM NDI suspension saturated with coronene in order to maintain constant NDI concentration throughout the experiments. Fluorescence titrations with TRGO were prepared by the same method mentioned above.

TRGO suspension was sonicated to promote layer separation of the TRGO until the mixture became homogeneous. The excess of TRGO was, then, allowed to settle.

4.6. X-ray crystallography

Experimental details relating to the single-crystal X-ray crystallographic study are summarised in Table **S1** and **S2**. Data for complex D-**3**·CHCl$_3$ were acquired using an Agilent Supernova Dual diffractometer equipped with an EosS2 CCD plate detector using a mirror monochromator (Cu Kα radiation, λ = 1.54184 Å). Data for complex L-**3**·C$_6$F$_6$ were acquired using a Bruker SMART diffractometer using a graphite monochromator (synchrotron radiation, λ = 0.6943 Å). For space group determination, structure solution and full-matrix least-squares refinement the WINGX-v2014 suite of programs was used.[75] All non-hydrogen atoms were refined with anisotropic displacement parameters. C-H hydrogen atom were placed onto calculated positions and refined riding on their parent atom. All hetero atom hydrogen atoms have been located in the difference Fourier map and were refined freely. The program MERCURY [76] was employed for the graphics used in this publication.

4.6. Preparation of samples for TCSPC Experiments

Samples for TCSPC experiments were prepared by the same method as those for fluorescence titration experiments differing only in that NDI and coronene concentrations were at 50 μM and 100 μM respectively.

Supporting Information

Electronic Supplementary Information (ESI) available: X-ray data for D-**3**.CD$_3$Cl and L-**3**.C$_6$F$_6$, heteronuclear NMR spectra, UV-Vis, Fluorescence spectroscopy, TCSPC analysis, SEM, TEM and CD. See DOI: 10.1039/x0xx00000x CCDC 1425604, 1436728 and 1457563 contain the supplementary crystallographic data for D-**3**·CHCl$_3$, L-**3**·C$_6$F$_6$ and L-**7**·NMP respectively. These data can be obtained free of charge via http://www.ccdc.cam.ac.uk/conts/retrieving.html, or from the Cambridge Crystallographic

Data Centre, 12 Union Road, Cambridge CB2 1EZ, UK; fax: +44 1223 336033; or e-mail:

deposit@ccdc.cam.ac.uk.

Received: ((will be filled in by the editorial staff))
Revised: ((will be filled in by the editorial staff))

Thermally Reduced Graphene Oxide Nanohybrids of Chiral Functional Naphthalenediimides for Prostate Cancer Cells Bioimaging

Keyword: Thermally reduced graphene oxide, naphthalenediimides, surface functionalization, hybrid materials, bioimaging probe.
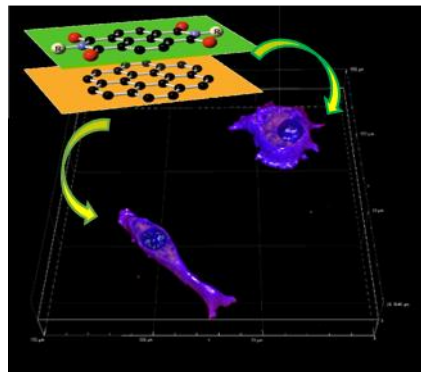
Halogenated amino acids within the naphthalenediimide (NDI) moieties can positively influence the degree of surface binding when designing functional nanomaterials. The non-covalent functionalization of planar carbon systems such as thermally reduced graphene oxide and coronene by using amino acid tagged NDIs is here reported and its potential as a prostate cancer bioimaging agent investigated via Fluorescence microscopy, UV-Vis, Fluorescence spectroscopy, NMR, CD, TCSPC, SEM, TEM and EDX.

James A. Tyson,[a] Vincenzo Mirabello,[a]* David G. Calatayud,[a] Haobo Ge,[a] Gabriele Kociok-Köhn,[b] Stanley W. Botchway,[c] G. Dan Pantoş,[a]* Sofia I. Pascu[a]*

J. A. Tyson, Dr. V. Mirabello, Dr. David G. Calatayud, Dr. Haobo Ge, Dr. G. Dan Pantoş, Dr. Sofia I. Pascu.

a. Department of Chemistry, University of bath, Claverton Down, BA2 7AY, UK

Dr. Gabriele Kociok-Köhn

b. Chemical Characterisation and Analysis Facility (CCAF), University of Bath, Claverton Down, BA2 7AY, UK

Prof. Stanley W. Botchway

c. Central Laser Facility, Rutherford Appleton Laboratory, Research Complex at Harwell, STFC Didcot OX11 0QX, UK

[1] E. H. L. Falcao, F. Wudl *J. Chem. Technol. Biotechnol*. **2007**, 82, 524-531.

[2] S. V. Morozov, K. S. Novoselov, M. I. Katsnelson, F. Schedin, D. C. Elias, J. A. Jaszczak, A. K. Geim *Phys. Rev. Lett*. **2008**, 100, 016602.

[3] A. A. Balandin, S. Ghosh, W. Bao, I. Calizo, D. Teweldebrhan, F. Miao, C. N. Lau *Nano Lett*. **2008**, 8, 902-907.

[4] C. Lee, X. Wei, J. W. Kysar, J. Hone *Science* **2008**, 321, 385-388.

[5] Y. Zhu, S. Murali, W. Cai, X. Li, J. W. Suk, J. R. Potts, R. S. Ruoff *Adv. Mater*. **2010**, 22, 3906-3924.

[6] Y. Shao, J. Wang, H. Wu, J. Liu, I. A. Aksay, Y. Lin *Electroanal*. **2010**, 22, 1027-1036.

[7] G. Eda, M. Chhowalla *Adv. Mater*. **2010**, 22, 2392-2415.

[8] F. Bonaccorso, Z. Sun, T. Hasan, A. C. Ferrari *Nat Photon*. **2010**, 4, 611-622.

[9] D. G. C. James A. Tyson, Vincenzo Mirabello, Boyang Mao, Sofia I. Pascu1 in *Labeling of Graphene, Graphene Oxides, and of Their Congeners: Imaging and Biosensing Applications of Relevance to Cancer Theranostics, Vol. doi:10.1016/bs.adioch.2015.09.007* (Ed. M. Bhuvaneswari), Elsevier Inc., **2015**.

[10] D. R. Dreyer, S. Park, C. W. Bielawski, R. S. Ruoff *Chem. Soc. Rev*. **2010**, 39, 228-240.

[11] Y. YeoHeung, D. Zhongyun, N. S. Vesselin, J. S. Mark *Nanotechnology* **2007**, 18, 465505.

[12] Q. Sheng, M. Wang, J. Zheng *Sensors and Actuat B-Chem*. **2011**, 160, 1070-1077.

[13] Z. Zhu, L. Garcia-Gancedo, A. J. Flewitt, H. Xie, F. Moussy, W. I. Milne *Sensors* **2012**, 12, 5996-6022.

[14] B. P. Corgier, F. Li, L. J. Blum, C. A. Marquette *Langmuir* **2007**, 23, 8619-8623.

[15] Z. Liu, J. T. Robinson, X. Sun, H. Dai *J. Am. Chem. Soc*. **2008**, 130, 10876-10877.

[16] S. Y. Lim, J. Ahn, J. S. Lee, M.-G. Kim, C. B. Park *Small* **2012**, 8, 1994-1999.

[17] L. Zhang, J. Xia, Q. Zhao, L. Liu, Z. Zhang *Small* **2010**, 6, 537-544.

[18] X. Shi, H. Gong, Y. Li, C. Wang, L. Cheng, Z. Liu *Biomaterials*. **2013**, 34, 4786-4793.

[19] Q. Chen, T. Chen, G.-B. Pan, H.-J. Yan, W.-G. Song, L.-J. Wan, Z.-T. Li, Z.-H. Wang, B. Shang, L.-F. Yuan, J.-L. Yang *Proc. Natl. Acad. Sci*. **2008**, 105, 16849-16854.

[20] M. Gallego, J. Calbo, J. Aragó, R. M. Krick Calderon, F. H. Liquido, T. Iwamoto, A. K. Greene, E. A. Jackson, E. M. Pérez, E. Ortí, D. M. Guldi, L. T. Scott, N. Martín *Angew. Chem.* **2014**, 126, 2202-2207.

[21] P. Lazar, F. Karlický, P. Jurečka, M. Kocman, E. Otyepková, K. Šafářová, M. Otyepka *J. Am. Chem. Soc*. **2013**, 135, 6372-6377.

[22] M. Gallego, J. Calbo, J. Aragó, R. M. Krick Calderon, F. H. Liquido, T. Iwamoto, A. K. Greene, E. A. Jackson, E. M. Pérez, E. Ortí, D. M. Guldi, L. T. Scott, N. Martín *Angew. Chem. Int. Ed.* **2014**, 53, 2170-2175.

[23] H. E. Katz, A. J. Lovinger, J. Johnson, C. Kloc, T. Siegrist, W. Li, Y. Y. Lin, A. Dodabalapur *Nature* **2000**, 404, 478-481.

[24] P. Mukhopadhyay, Y. Iwashita, M. Shirakawa, S.-i. Kawano, N. Fujita, S. Shinkai *Angew. Chem. Int. Ed.* **2006**, 45, 1592-1595.

[25] W. W. Stewart *Nature* **1981**, 292, 17-21.

[26] D. A. Vicic, D. T. Odom, M. E. Núñez, D. A. Gianolio, L. W. McLaughlin, J. K. Barton *J. Am. Chem. Soc*. **2000**, 122, 8603-8611.

[27] H. N. Lee, Z. Xu, S. K. Kim, K. M. K. Swamy, Y. Kim, S.-J. Kim, J. Yoon *J. Am. Chem. Soc*. **2007**, 129, 3828-3829.

[28] C. Oelsner, C. Schmidt, F. Hauke, M. Prato, A. Hirsch, D. M. Guldi *J. Am. Chem. Soc*. **2011**, 133, 4580-4586.

[29] K. Dirian, S. Backes, C. Backes, V. Strauss, F. Rodler, F. Hauke, A. Hirsch, D. M. Guldi *Chem. Sci*. **2015**, 6, 6886-6895.